DEVELOPMENT OF COBALT NANOPARTICLES SUPPORTED ON ALUMINA CATALYSTS USING FLAME SPRAY PYROLYSIS FOR FTS REACTION

By

Naphaphan Kunthakudee

A Thesis Submitted in Partial Fulfillment of the Requirements for the Degree

MASTER OF ENGINEERING

Department of Chemical Engineering

Graduate School

SILPAKORN UNIVERSITY

2010

DEVELOPMENT OF COBALT NANOPARTICLES SUPPORTED ON ALUMINA CATALYSTS USING FLAME SPRAY PYROLYSIS FOR FTS REACTION

By

Naphaphan Kunthakudee

A Thesis Submitted in Partial Fulfillment of the Requirements for the Degree
MASTER OF ENGINEERING
Department of Chemical Engineering
Graduate School
SILPAKORN UNIVERSITY
2010

การพัฒนาตัวเร่งปฏิกิริยาโคบอลต์ที่มีอนุภาคขนาดนาโนบนตัวรองรับอะลูมินาด้วยเฟลมสเปรย์ไพโรไลซิสสำหรับปฏิกิริยาการสังเคราะห์ฟิชเชอร์โทรป

โดย

นางสาวนภาพรรณ คันธกุฎี

วิทยานิพนธ์นี้เป็นส่วนหนึ่งของการศึกษาตามหลักสูตรปริญญาวิศวกรรมศาสตรมหาบัณฑิต

สาขาวิชาวิศวกรรมเคมี

ภาควิชาวิศวกรรมเคมี

บัณฑิตวิทยาลัย มหาวิทยาลัยศิลปากร

ปีการศึกษา 2553

The Graduate School, Silpakorn University has approved and accredited the Thesis title of “Development of Cobalt Nanoparticles Supported on Alumina Catalysts Using Flame Spray Pyrolysis for FTS Reaction” submitted by Miss Naphaphan Kunthakudee as a partial fulfillment of the requirements for the degree of Master’s of Chemical Engineering.

.....
(Assistant Professor Panjai Tantatsanawong ,Ph.D.)
Dean of Graduate School
...../...../.....

The Thesis Advisor

1. Assistant Professor Choowong Chaisuk, D.Eng.
2. Kajornsak Faungnawakij, Ph.D.

The Thesis Examination Committee

..... Chairman
(Assistant Professor Okorn Mekasuwandumrong, D.Eng.)
...../...../.....

..... Member
(Assistant Professor Joongjai Panpranot, Ph.D.)
...../...../.....

..... Member
(Veerayut Lersbamrungsuk, D.Eng.)
...../...../.....

..... Member
(Assistant Professor Choowong Chaisuk, D.Eng.)
...../...../.....

..... Member
(Kajornsak Faungnawakij, Ph.D.)
...../...../.....

52404207 : MAJOR : CHEMICAL ENGINEERING
KEY WORDS : FISCHER-TROPSCH SYNTHESIS/ FLAME SPRAY PYROLYSIS/ COBALT CATALYST/ NANOPARTICLES
NAPHAPHAN KUNTHAKUDEE : DEVELOPMENT OF COBALT NANOPARTICLES SUPPORTED ON ALUMINA CATALYSTS USING FLAME SPRAY PYROLYSIS FOR FTS REACTION. THESIS ADVISORS : ASST.PROF.CHOOWONG CHAISUK, D.Eng., AND KAJORNSAK FAUNGNAWAKIJ, Ph.D.. 80 pp.

In this research, cobalt-based catalysts with 20 wt% Co and 0.5 wt% Ru supported on Al_2O_3 were prepared using flame spray pyrolysis (FSP) and their catalytic performance was studied for Fischer–Tropsch synthesis (FTS) in a fixed bed reactor at 220 °C and 1 atm. The particle sizes of all catalysts were in a range of 15-19 nm. FSP could provide the nanoparticle catalyst with narrow size distribution. The $CoAl_2O_4$ spinel phase was detected on the catalysts prepared by FSP. $CoAl_2O_4$ formed in FSP led to low reaction rate as compared with Co_3O_4 formed in an impregnation method. In addition, it was found that $CoAl_2O_4$ phase could promote long chain hydrocarbon (C_{10+}) formation while Co_3O_4 accelerated the formation of methane (CH_4). The addition of Ru to alumina-supported cobalt catalyst increased reducibility and dispersion of the cobalt species, and subsequently enhanced the reactivity of the catalyst. However, the presence of Ru did not inhibit the formation of $CoAl_2O_4$ during FSP synthesis. Interestingly, the product distribution could be selective to control by a combination of FSP and impregnation methods on the cobalt-based catalyst preparation.

Department of Chemical Engineering Graduate School, Silpakorn University Academic Year 2010
Student's signature .....
Thesis Advisors' signature 1. ..... 2. .....

52404207 : สาขาวิชาวิศวกรรมเคมี
คำสำคัญ : ปฏิกิริยาการสังเคราะห์ฟิชเชอร์โทรป/ เฟลมสเปรย์ไพโรไลซิส/ ตัวเร่งปฏิกิริยาโคบอลต์/ อนุภาคขนาดนาโน

นภาพรรณ คันธกุฎี : การพัฒนาตัวเร่งปฏิกิริยาโคบอลต์ที่มีอนุภาคขนาดนาโนบนตัวรองรับอะลูมินาโดยเทคนิคเฟลมสเปรย์ไพโรไลซิสสำหรับปฏิกิริยาการสังเคราะห์ฟิชเชอร์โทรป อาจารย์ที่ปรึกษาวิทยานิพนธ์ : ผศ.ดร.ชูวงศ์ ชัยสุข และ ดร.ขจรศักดิ์ เฟื่องนวกิจ 80 หน้า

ในงานวิจัยนี้ ทำการเตรียมตัวเร่งปฏิกิริยาที่มี 20 เปอร์เซ็นต์โดยน้ำหนักของโคบอลต์และ 0.5 เปอร์เซ็นต์โดยน้ำหนักของรูทีเนียมบนตัวรองรับอะลูมินาด้วยเฟลมสเปรย์ไพโรไลซิส และศึกษาประสิทธิภาพของการเร่งปฏิกิริยาการสังเคราะห์ฟิชเชอร์โทรปในเครื่องปฏิกรณ์แบบเบดนิ่งที่อุณหภูมิ 220 องศาเซลเซียสและความดัน 1 บรรยากาศ ขนาดอนุภาคของตัวเร่งปฏิกิริยาทั้งหมดอยู่ในช่วง 15-19 นาโนเมตร เฟลมสเปรย์ไพโรไลซิสสามารถเตรียมตัวเร่งปฏิกิริยาที่มีอนุภาคขนาดนาโนด้วยการกระจายตัวของขนาดที่แคบ พบเฟสโคบอลต์อะลูมิเนตบนตัวเร่งปฏิกิริยาที่เตรียมด้วยเฟลมสเปรย์ไพโรไลซิส โคบอลต์อะลูมิเนตที่เกิดขึ้นในเฟลมสเปรย์ไพโรไลซิสทำให้อัตราการเกิดปฏิกิริยาที่ต่ำเมื่อเปรียบเทียบกับโคบอลต์ออกไซด์ที่เกิดขึ้นด้วยวิธีการเคลือบฝัง นอกจากนี้พบว่า เฟสโคบอลต์อะลูมิเนตสามารถส่งเสริมการเกิดสารไฮโดรคาร์บอนสายโซ่ยาว (C_{10+}) ในขณะที่โคบอลต์ออกไซด์เร่งการเกิดมีเทน การเติมรูทีเนียมลงบนตัวเร่งปฏิกิริยาโคบอลต์บนตัวรองรับอะลูมินาช่วยเพิ่มความสามารถในการรีดิวซ์และการกระจายตัวของสปีชีส์โคบอลต์ และส่งผลให้เพิ่มการเกิดปฏิกิริยาของตัวเร่งปฏิกิริยา อย่างไรก็ตามการเติมรูทีเนียมไม่สามารถยับยั้งการเกิดโคบอลต์อะลูมิเนตระหว่างการสังเคราะห์ด้วยเฟลมสเปรย์ไพโรไลซิส เป็นที่น่าสนใจว่า สามารถเลือกที่จะควบคุมการกระจายตัวของผลิตภัณฑ์โดยการรวมกันของวิธีเฟลมสเปรย์ไพโรไลซิสและวิธีการเคลือบฝังบนการเตรียมตัวเร่งปฏิกิริยาโคบอลต์

ภาควิชาวิศวกรรมเคมี บัณฑิตวิทยาลัย มหาวิทยาลัยศิลปากร ปีการศึกษา 2553

ลายมือชื่อนักศึกษา.....

ลายมือชื่ออาจารย์ที่ปรึกษาวิทยานิพนธ์ 1. ..... 2. .....

ACKNOWLEDGEMENTS

The author would like to express her sincere gratitude and appreciation to her advisor, Assistant Professor Choowong Chaisuk, D.Eng. and co advisor, Dr. Kajornsak Faungnawakij for providing guidance and valuable advice throughout this research and devotion to revise this thesis. Futhermore, we are similarly grateful for suggestion and helpful that we have received from Assistant Professor Okorn Mekasuwandumrong, D.Eng..

In particular, the author would also be grateful to Assistant Professor Okorn Mekasuwandumrong, as the chairman, Dr. Veerayut Lersbamrungsuk and Assistant Professor Joongjai Panpranot as the members of the thesis committee. The author would like to thank the Center of Excellence on Catalysis and Catalytic Reaction Engineering, Department of Chemical Engineering, Faculty of Engineering, Chulalongkorn university and National Nanotechnology Center (NANOTEC) for the instrument supports. The author would like to thank Silpakorn University Research and Development Institute (SURDI), the Thailand Research Fund (TRF) and National Science and Technology Development Agency (NSTDA) (Project No.TGIST 01-53-057) for the financial supports.

Most of all, the author would like to express her highest gratitude to her parents who always pay attention to us all the time for suggestions, supports and encourangements. The most success of graduation is devoted to her parents.

Finally, Many thanks for kind suggestions and useful help to Mr. Narongrat Poovarawan, the members of the Center of Excellence on Catalysis and Catalytic Reaction Engineering, Department of Chemical Engineering, Faculty of Engineering, Chulalongkorn university and Mr. Veeraprach Kongthong, the members of Department of Chemical Engineering, Faculty of Engineering, Kasetsart university for their assistances.

TABLE OF CONTENTS

LIST OF TABLES

LIST OF FIGURES

Figures Page

CHAPTER 1

INTRODUCTION

Nowadays oil prices have been high and tend to continuously increase and fuel consumption remains a serious problem. Many researchers attempt to find a new source for fuel that is not only renewable, but also better for the environment. Fischer–Tropsch synthesis (FTS) is a part of gas-to-liquids (GTL) technology, which produces synthetic liquid hydrocarbons from natural gas and it is free of sulfur and aromatics pollutants [1]. FTS reaction occurs in a state require catalysts. A key step in improving the activity of FTS is the development of highly active catalysts [2, 3].

The cobalt-based catalysts are the preferred catalysts in FTS for the direct conversion of syngas because of high activity, high selectivity for long-chain paraffins used as synthetic diesel, low activity for the water gas shift (WGS) reaction, more stable toward deactivation by water (a byproduct of FTS) [4]. In the FTS process it has been shown that both catalyst activity and hydrocarbon selectivity are function of the density of surface active sites (Co^0), and at the same time depend on both cobalt dispersion and reducibility. These two parameters are mainly determined by the cobalt-support interaction strength. In order to achieve a high density of metal sites (Co^0), cobalt precursors are usually dispersed on porous carriers, such as amorphous Al_2O_3, SiO_2, or TiO_2 [5]. The support shows the different metal-support interaction, which relates to catalytic activity of FTS.

Al_2O_3 is one of the most employed supports for cobalt FTS catalyst because of its favorable mechanical properties and adjustable surface properties. However, the strong interaction between the supported cobalt and the alumina supports often results in the relative low reducibility [6]. The former has significant interaction with the supported cobalt oxides, contributing to the formation of a smaller support-metal cluster and limited reducibility due to the strong interaction by the diffusion of the cobalt ion into the structure of alumina.

Usually noble metals are used as promoters of supported Co catalysts. Promoters such as Pt, Re and Ru have been using extensively to enhance the reducibility of cobalt oxide, which is otherwise limited by a strong interaction between the oxides and the supports [7]. Ru acts as a source of hydrogen spillover, helps increase the reducibility of Co species, preserves activity by preventing the buildup of carbonaceous deposits and exhibits cluster and ligand effects [7]. Supported Ru catalysts are excellent FTS catalysts with high activity and chain growth probability. Indeed, supported ruthenium catalysts for FTS produce C_{5+} hydrocarbons with a selectivity of over 90% at temperatures as low as 100 °C. The application of Ru catalyst in the FTS is restricted due to its high price. Therefore, usually a small amount of ruthenium is used as a promoter for the supported cobalt catalyst [8].

Various aerosol reactors and methods have been developed for the synthesis of a wide variety of metal and metal oxide particles. Compared to wet-chemical routes with various post-treatment steps, such as filtration, washing, drying and calcination, gas-phase processes allow the preparation of the desired material without any further post-processing. Flame technology is a scalable, continuous and well-established method for the production of nanoparticles in large quantities. Flame processes for catalyst preparation also have the advantage that multicomponent forms of catalysts can be readily prepared and their mixing can be controlled to obtain different distributions to prepare tailormade nanocomposites. Morever, it can be made various nanopowders with high production rate [9, 10]. In general, flame-made materials are non-porous with a high external surface area that went through high temperatures and cooling rates, resulting in some unique phases and good thermal stability and mass transfer during catalysis

Flame spray pyrolysis (FSP) processes are quite attractive. They can employ a wide array of precursors for synthesis of a nanoparticles as each droplet contains the precursor in the same stoichiometry as desired in the product. The process features short residence times (a few milliseconds) and high maximum process temperatures (up to 2700 °C) [10]. The main advantage of FSP is the formation of generally homogeneous, nano-sized particles through control of the precursor-solvent

composition. Up till now a variety of products have been synthesized by FSP, for example, zinc oxide, alumina, magnesium-aluminate, titania, zirconia, etc.

In this work, we have investigated the catalytic performance of Co nanoparticle supported on alumina catalyst using flame spray pyrolysis and the effect of ruthenium promoter for production of synthetic fuel by Fischer-Tropsch systhesis

Objective of the Research

The purpose of this work is to develop of cobalt nanoparticle supported on alumina catalyst using flame spray pyrolysis for Fischer-Tropsch systhesis.

Scope of the Research

1 Development of catalysts

1.1 Study of the characteristics and the catalytic performance of Co supported on alumina catalysts (range 10-20% Co loading), which were prepared by

- Flame spray pyrolysis technique (FSP)
- Impregnation method
- Combination of FSP and impregnation

1.2 Study of the effect of Co content in the supported catalysts prepared by three methods on the characteristics and catalytic performance of Co catalysts for Fischer-Tropsch systhesis

1.3 Study of the effect of Ru promoter on the characteristics and catalytic performance of Co catalysts for Fischer-Tropsch systhesis

2 Catalyst characterization

2.1 The bulk crystal structure and chemical phase composition are determined by X-ray diffraction (XRD).

2.2 The surface area of support and catalysts, the average pore sizes diameter and the pore size distribution are determined by N_2 physisorption.

2.3 The crystallite sizes are observed using transmission electron microscopy (TEM).

2.4 Reducibility of catalysts are determined by temperature programmed reduction (TPR).

2.5 The relative amounts of active cobalt metals on the catalyst samples are calculated from H_2 chemisorption.

2.6 The surface composition of the catalysts are determined from X-ray photoelectron spectroscopy (XPS).

3 Catalytic evaluation

The catalytic activity of Co supported on alumina catalysts is tested by Fischer-Tropsch synthesis. This reaction was carried out at 220 °C and 1 atm in micro tubular reactor. The reactant feed consisted of H_2 and CO at H_2/CO ratio of 2.33. The effluent products were analyzed by two GCs connecting with TCD and FID.

CHAPTER 2

LITERATURE REVIEWS

2.1 Fischer-Tropsch Synthesis

H. Xiong et al. [11] studied the effect of Al_2O_3 porosity on the performance of Co/Al_2O_3 catalyst for Fischer-Tropsch synthesis (FTS). Al_2O_3 was calcined at different temperature to get the support with different pore size. Co/Al_2O_3 catalysts with different pore size were prepared by incipient wetness impregnation technique. The pore size of support Al_2O_3 was found to have a significant effect on Co_3O_4 crystallite diameter, catalyst reducibility and FTS activity. The larger pore size enhanced the formation of bigger crystallite diameter Co_3O_4 on the catalyst and the occurrence of larger pore size catalyst decreased the number of cobalt active sites on the surface of the catalyst and the reducibility of the catalyst, resulting in the decrease in FTS activity. The $CoAl_2O_4$ spinel phase was detected on the prepared catalysts by incipient wetness impregnation and its content on the catalysts decreased with the increase of zirconium loading, indicating that Zr-added could inhibit $CoAl_2O_4$ formation [12]. The addition of zirconium to the Co catalyst caused the increase of cobalt cluster size. Zr addition has been shown to improve the activity and C_{5+} selectivity of Co/Al_2O_3 catalyst for Fischer–Tropsch synthesis. This could be explained by the increase of active metal cobalt site and reducibility.

Burakorn et al. [13] studied the physicochemical properties of cobalt dispersed on mixed nano-Al_2O_3-ZrO_2 supports. The samples were prepared by impregnation of the cobalt precursor onto the various mixed nano-Al_2O_3–ZrO_2 supports. The reaction study was also performed in order to measure activity and product selectivity towards CO hydrogenation. The resulted reaction study is also shown in Table 1.

Table 2.1 Reaction rates and product selectivity of Co/Al_2O_3-ZrO_2 catalysts [13]

Sample	Rate (μmol/g cat)	Product Selectivity (%)		
		C_1	C_2-C_3	C_4-C_5
Co/Al-100-Zr-0	0.4	99.4	0.6	-
Co/Al-80-Zr-20	0.4	99.1	0.9	-
Co/Al-60-Zr-40	0.2	90.8	6.5	2.7
Co/Al-40-Zr-60	0.2	90.4	6.8	2.8
Co/Al-20-Zr-80	0.2	91.4	5.4	3.2
Co/Al-0-Zr-100	0.3	95.6	3.2	1.2

Considering the selectivity of product, it showed that the selectivity to methane (C_1) essentially decreased with the amounts of nano-ZrO_2 added in the mixed supports. On the other hand, more amounts of longer chain hydrocarbons (C_2–C_5) can be obtained with the presence of the nano-ZrO_2 in the mixed supports. It was known that CO hydrogenation was a kind of polymerization reactions where insertion of the –CH_2– (methylene group) occurred through the active center. Thus, the product distribution strongly depended on the nature of active centers, rate of propagation and rate of termination. Obviously, the termination of chain growth occurred and was recognized as the chain growth probability. It can be concluded that the presence of the nano-ZrO_2 in the mixed supports apparently enhanced the chain growth probability. As a matter of fact, it can result in the observation of longer chain hydrocarbons even at the specified methanation condition where the high ratio of H_2/CO (10/1) was applied. Based on the use of pure nano-ZrO_2 as a support, the similar trend regarding the effect of nano-ZrO_2 on the chain growth probability was also observed.

The important point in the development of FTS was the improvement of the catalyst activity and selectivity by increasing the number of active Co metal sites that were stable during reduction and under reaction conditions. The effect of reduction procedure on catalyst properties, activity and products selectivity of ruthenium-promoted Co/γ-Al_2O_3 catalyst in Fischer-Tropsch synthesis (FTS) was investigated.

Catalyst samples were reduced with different reduction gas compositions and passivated before being characterized. Different activity and product selectivity analysis were also performed. These results showed that the catalyst dispersion, the particle size, and the degree of reduction changed with different reduction gas compositions, which were resulted from the water partial pressures in reduction process that gave various degrees of interaction with the support. It has been suggested that the FTS activity of cobalt catalyst was directly dependent on the catalyst reducibility. A reduction gas with a molar ratio of H_2/He = 1 was used to prevent the formation of Co-support compound during catalyst reduction.

Hosseini et al. [15] investigated the ruthenium promoted cobalt alumina catalysts prepared by co-impregnation method. The selected Ru loadings were 0.5, 1.0, 1.5 and 2.0 wt%, while the loading of Co was 20 wt% in all prepared samples. Characterization studies of catalysts promoted with 0.5% and 1.0% Ru showed higher extent of reduction, as well as, better dispersion of Co on the support, reduction of particle size of the metal, and of pore volume of catalysts. These catalysts also exhibited higher CO conversions. By further increasing of the Ru content (1.5 and 2 wt %); however, the results were reversed including the extents of reduction of Co and CO conversion was decreased. However, the C_{5+} selectivity of the products was remained rather unaffected. Meanwhile, the catalysts showed higher selectivity on C_5–C_{12} hydrocarbons.

Li et al. [16] studied the formation of metal nanoparticles during the incipient wetness synthesis process for both Ru-promoted and non-promoted Co/γ-Al_2O_3 catalysts. It was found that the addition of Ru promoted the formation of individual CoRu bimetallic nanoparticles and enhanced the reducibility of small Co particles. In situ EELS nano-analysis showed that Co existed in metallic form only in the small 1–3 nm bimetallic CoRu particles. This suggested that Ru enhanced the formation of metallic Co. The presence of the small metallic particles in the Co-Ru/Al_2O_3 catalyst increased the reducibility of the surface metal atoms, thus enhancing catalyst activity.

2.2 Flame Spray Pyrolysis

Currently, catalysts are mostly manufactured using wet-chemical techniques. Incipient wetness impregnation, sol-gel, precipitation, grafting and solid-state reactions are batch processes requiring several aftertreatment steps, such as filtration, drying and calcination. Flame technology is a scalable, continuous and well-established method for production of nanoparticles in large quantities. Since the 1970s, flame-made materials have been used as catalyst supports (i.e. Al_2O_3, SiO_2, TiO_2) and as photocatalysts (mainly TiO_2) [17].

Flame spray pyrolysis (FSP), a flame-assisted liquid droplet-to-particle conversion process, has been of interest to produce single and multi component nanoparticles with an advantage of starting with solution of precursors [18]. The nanoparticles generated by the FSP have shown high purity, controlled stoichiometry and crystallinity because the flame could be maintained at temperatures high enough to complete thermal decompositions through intense oxidation.

In FSP the metal precursor was a combustible liquid that was sprayed and ignited, resulting in product nanoparticles. The organic precursor solution was dispersed either ultrasonically or by gas convection through a nozzle forming a fine spray which was ignited. The metal precursors evaporated in this spray flame and were combusted. Particles are then formed by nucleation from the gas phase. The process featured short residence times (a few milliseconds) and high maximum process temperatures (up to 3000 K) [19]. This method was developed as early 1977 by Sokolowski et al. [20] for the synthesis of Al_2O_3. Flame-made particles were collected with the aid of filters, cyclones or electrostatic precipitators. Alternatively, instead of collecting the flame products, they can be deposited directly on a flat plate, tube, fibre or foam substrate [21].

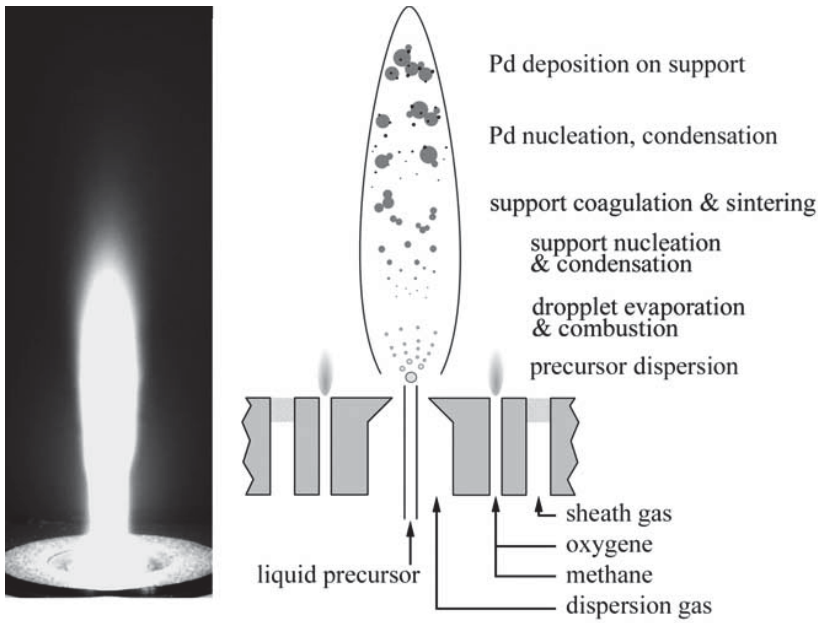

Figure 2.1 Sketch of the flame spray pyrolysis unit. The image shows a typical spray flame producing Pd/Al_2O_3 nanoparticles [22].

Production rates of these materials can be of the order of 25 t/h and the corresponding reactors resemble best the rockets of a departing space shuttle [23]. The main advantage of FSP was the formation of generally homogeneous, nano-sized particles through control of the precursor-solvent composition [24]. FSP has been used for the synthesis of many different solid catalysts, such as Pt/Al_2O_3 [25] and Pd/Al_2O_3.

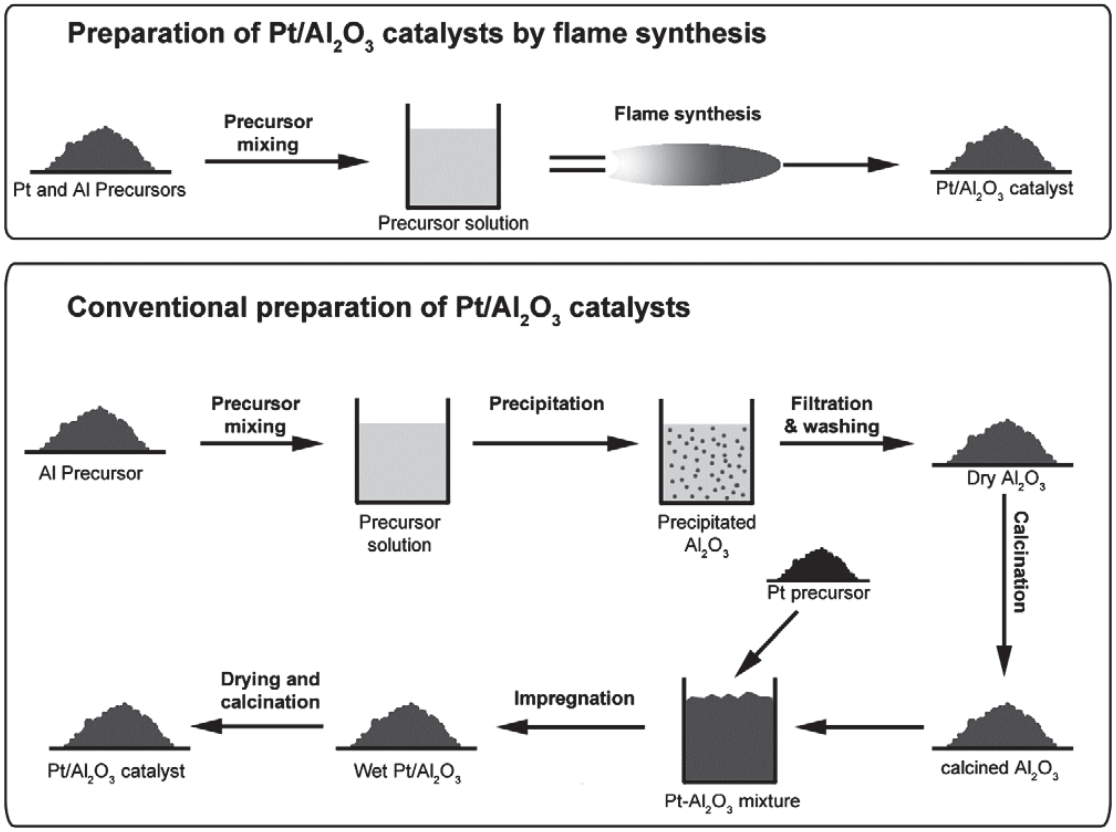

Figure 2.2 Comparison of conventional wet-phase and flame methods for the synthesis of catalysts as illustrated for Pt/Al_2O_3. Flame synthesis allows preparation of the catalyst in one step, whereas the conventional route by precipitation and impregnation is a multi-step process [19].

In the conventional flame synthesis where vapor phase reaction was employed, the amount of precursor introduced into the flame determined the collision frequency of the particles during the growth process. Chang et al. [26] investigated an increment in precursor concentration leading to increase the particle size because of the enhanced collision and sintering rates at the high flame temperature. Similarly, higher precursor concentrations resulted in larger particle sizes in the flame spray pyrolysis. TEM micrographs of TiO_2 nanoparticles are shown in Figure 3 at various precursor concentrations. Particles were spherical and non-hollow. The particle size distributions obtained from the TEM micrographs are also shown in Figure 2.3. The geometric mean diameter and geometric standard deviation of particles prepared at the precursor concentration of 0.1 M were about 9 nm and 1.48, respectively, and

those were increased to about 49 nm and 1.83 by increasing the precursor concentration to 1.0 M. The size of particles prepared with low precursor concentration was clearly smaller than that of particles prepared with high precursor concentration.

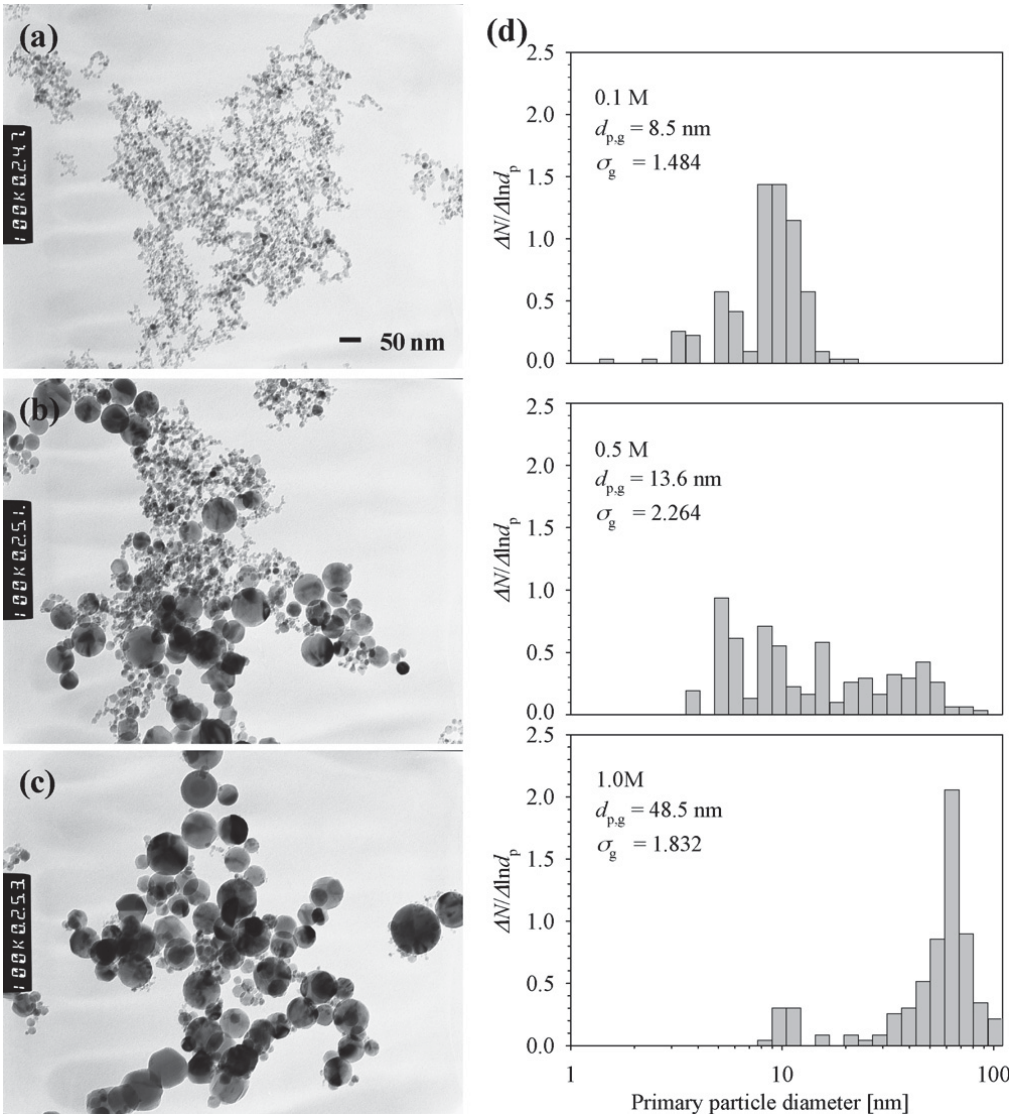

Figure 2.3 TEM micrographs (a–c) and particle size distribution (d) of TiO_2 nanoparticles prepared at various precursor concentrations: (a) 0.1 M, (b) 0.5 M and (c) 1.0 M [26].

Besides, the effect of precursor feed rate on the particle morphology and size was investigated by increasing the precursor feed rate while keeping the pressure of dispersion air and the other gas flow rates at constant. Even though precursor feed rate increased, the morphology of powder kept spherical, non-hollow and non-aggregated, but particle size increased [27].

The average particle diameters were calculated from the specific surface areas measured by BET analysis and are shown in Figure 4. As the pressure of dispersion air increased from 1.0 to 5.0 kg_f/cm^2 at the fixed experimental conditions the specific surface areas of the silica nanoparticles were increased from 45.0 to 250.4 m^2/g and the corresponding average particle diameters were decreased from 60.7 to 10.9 nm. In addition, with an increment in the feed rate of precursor, the average particle size increased from 24.1 to 50.7 nm while keeping the other experimental variables at constant.

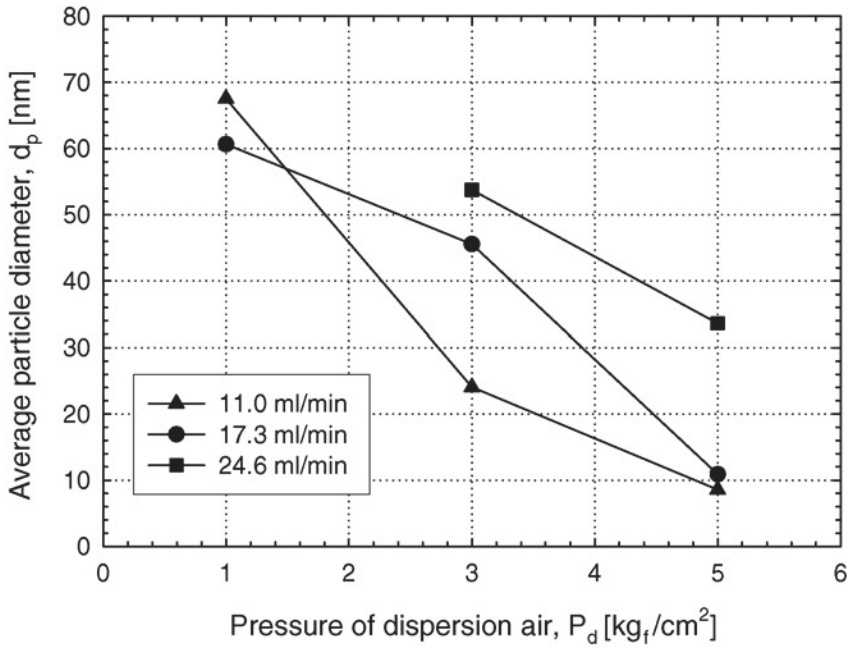

Figure 2.4 The average particle diameter of silica nanoparticles prepared by FSP at various pressures of dispersion air and feed rates of precursor [27].

CHAPTER 3

FISCHER-TROPSCH SYNTHESIS

The conversion of natural gas to hydrocarbons (Gas-To-Liquids route) is currently one of the most promising topics in the energy industry due to economic utilization of remote natural gas to environmentally clean fuels, specialty chemicals and waxes. Alternatively, coal or heavy residues can be used on sites where these are available at low costs. Coal and natural gas can be converted into synthesis gas, a mixture of predominantly CO and H_2, by either partial oxidation or steam reforming processes. Possible reactions of synthesis gas are shown in Figure 3.1.

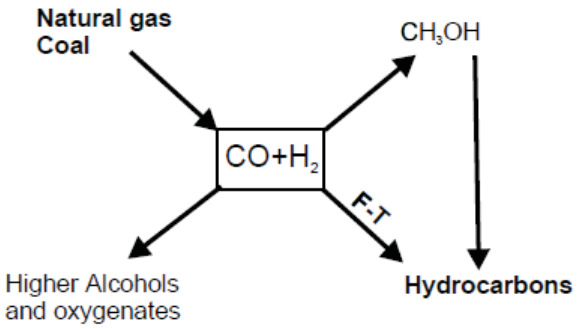

Figure 3.1 Possible reactions from synthesis gas [28]

The conversion of the synthesis gas to aliphatic hydrocarbons over metal catalysts was discovered by the German researchers, Franz Fischer and Hans Tropsch in 1923 [28]. They proved that CO hydrogenation over iron, cobalt or nickel catalysts at 180-250 °C and atmospheric pressure resulted in a product mixture of linear hydrocarbons. The Fischer-Tropsch product spectrum consists of a complex multicomponent mixture of linear and branched hydrocarbons and oxygenated products. Main products are linear parafins and olefins. The overall reactions of the Fischer-Tropsch synthesis are summarized in Table 3.1.

Table 3.1 Major overall reactions in the Fischer-Tropsch synthesis [28]

Main reactions	
1. Paraffins	$(2n+1)H_2 + nCO \rightarrow C_nH_{2n+2} + nH_2O$
2. Olefins	$2nH_2 + nCO \rightarrow C_nH_{2n} + nH_2O$
3. Water gas shift reaction	$CO + H_2O \rightleftarrows CO_2 + H_2$
Side reactions	
4. Alcohols	$2nH_2 + nCO \rightarrow C_nH_{2n+2}O + (n-1)H_2O$
5. Boudouard reaction	$2CO \rightarrow C + CO_2$
Catalyst modifications	
6. Catalyst oxidation/reduction	a. $M_xO_y + yH_2 \rightleftarrows yH_2O + xM$
	b. $M_xO_y + yCO \rightleftarrows yCO_2 + xM$
7. Bulk carbide formation	$yC + xM \rightleftarrows M_xC_y$

Figure 3.2 shows a block diagram of the overall Fischer-Tropsch process configuration. The commercial process involves three main sections, namely: synthesis gas production and purification, Fischer-Tropsch synthesis, and product grade-up. Synthesis gas can be obtained from reforming of natural gas with either steam or carbon dioxide, or by partial oxidation. Usually, a combination of synthesis gas production processes is used to obtain synthesis gas with a stoichiometric ratio of hydrogen and carbon monoxide.

The Fischer-Tropsch reaction is the chemical heart in the gas-to-liquid technology. The highly exothermic Fischer-Tropsch reaction converts synthesis gas into a large range of linear hydrocarbons [29], schematically represented as:

$$nCO + 2nH_2 \quad \rightarrow \quad -(CH_2)_n- \; + \; nH_2O \qquad\qquad \Delta H = -165\ kJ/mole$$

The Fischer-Tropsch synthesis section consists of FT reactors, recycle and compression of unconverted synthesis gas, removal of hydrogen and carbon dioxide, reforming of methane produced and separation of the FT products.

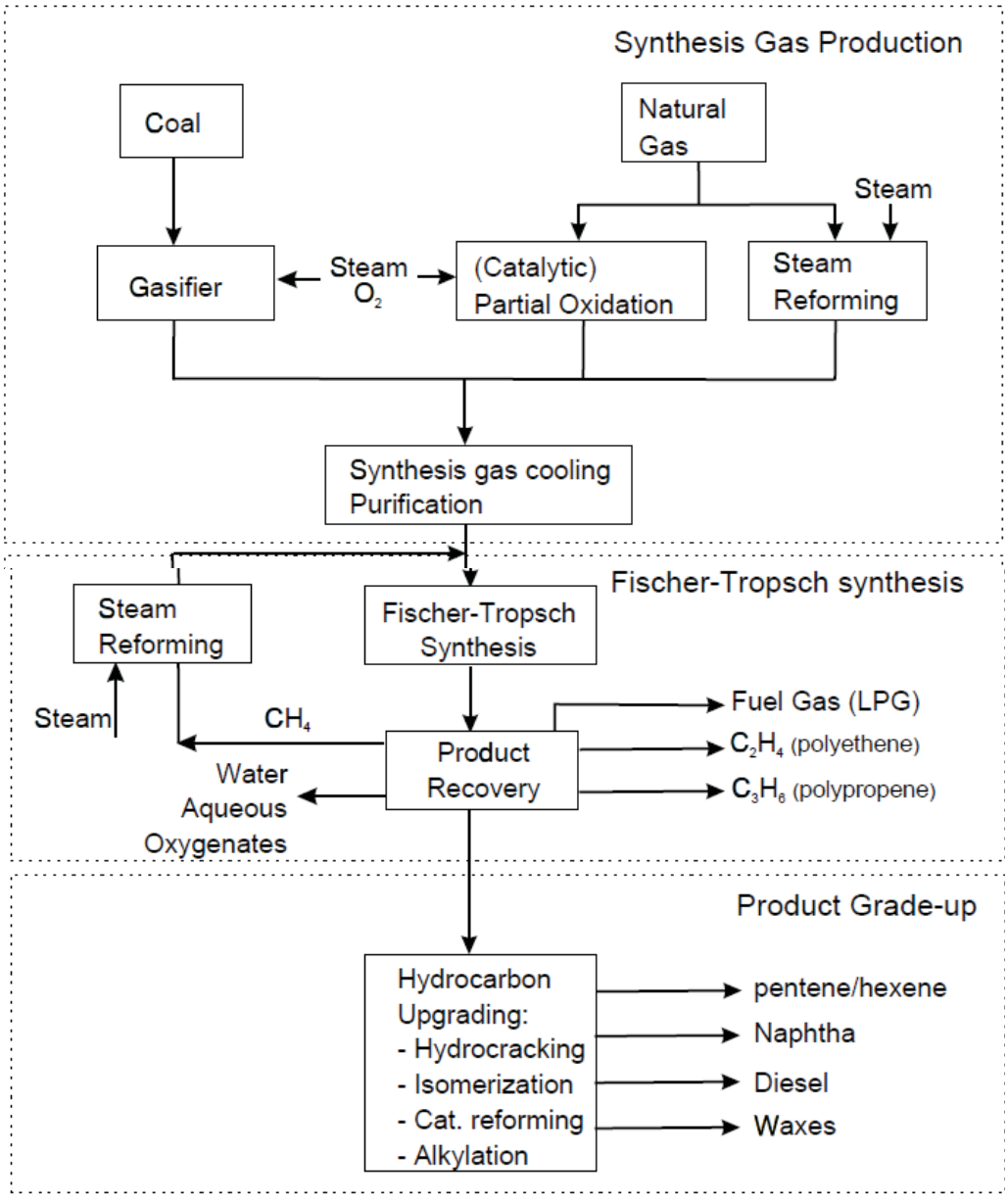

Figure 3.2 Overall process scheme Fischer-Tropsch synthesis [28]

The Fischer-Tropsch reaction that there is a reaction between surface methylene and surface hydrogen to form a surface methyl, and that chain growth is propagated by successive insertions of methylene into the metal-alkyl bond is shown in Figure 3.3. Termination of the chain growth takes place by means of a β-hydride elimination to give α-olefins or a reduction by surface hydride to give alkanes [30].

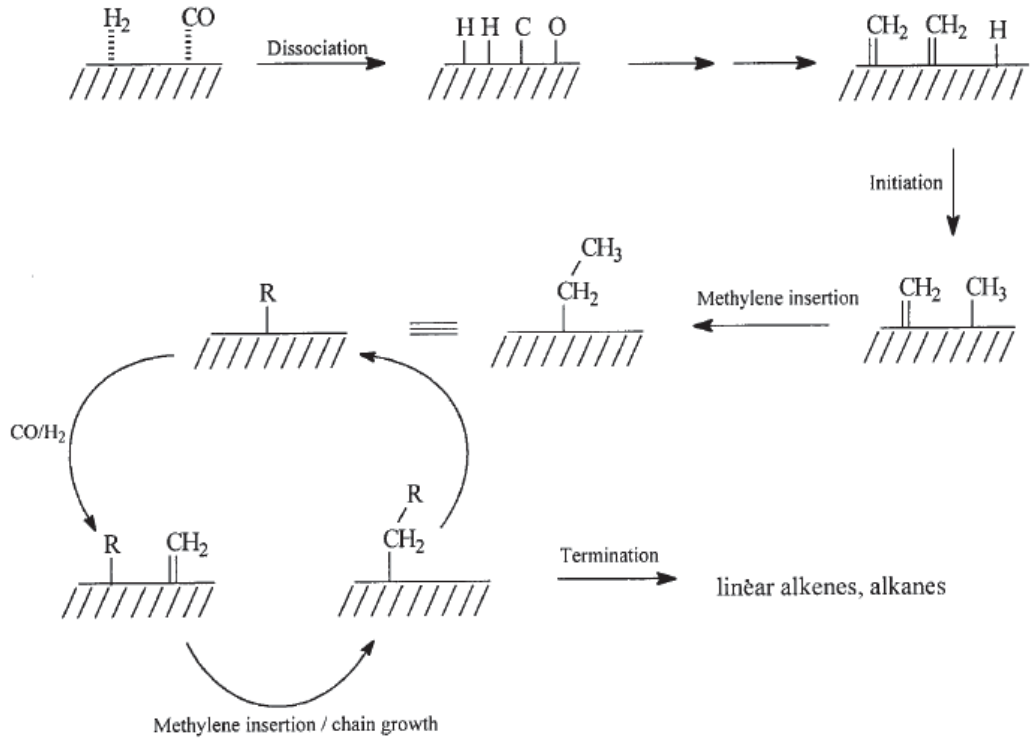

Figure 3.3 The mechanism for initiation and chain growth in the Fischer-Tropsch reaction [30]

In addition, methyl-branched species may also be formed as secondary products as oxygenated compounds produced in the Fischer-Tropsch reaction including alcohols, aldehydes, acids, and ketones. The majority of the products are linear with terminal functionality. The amounts and types of oxygenates formed are highly dependent on the catalyst and the reaction conditions, but typically on an iron based catalyst ethanol is the principle oxygenate formed, followed by methanol, *n*-propanol, and acetic acid [31]. Oxygenates in the Fischer-Tropsch reaction may be formed through a CO insertion reaction with a surface alkyl species to form a surface acyl species as shown in Figure 3.4. Acyl compounds of Fischer-Tropsch active metals were synthesized [32, 33] and characteristic acyl bands were identified by in situ IR studies [34]. Alcohols and aldehydes could be formed as a result of the partial reduction of the acyl species by surface hydrogen [35].

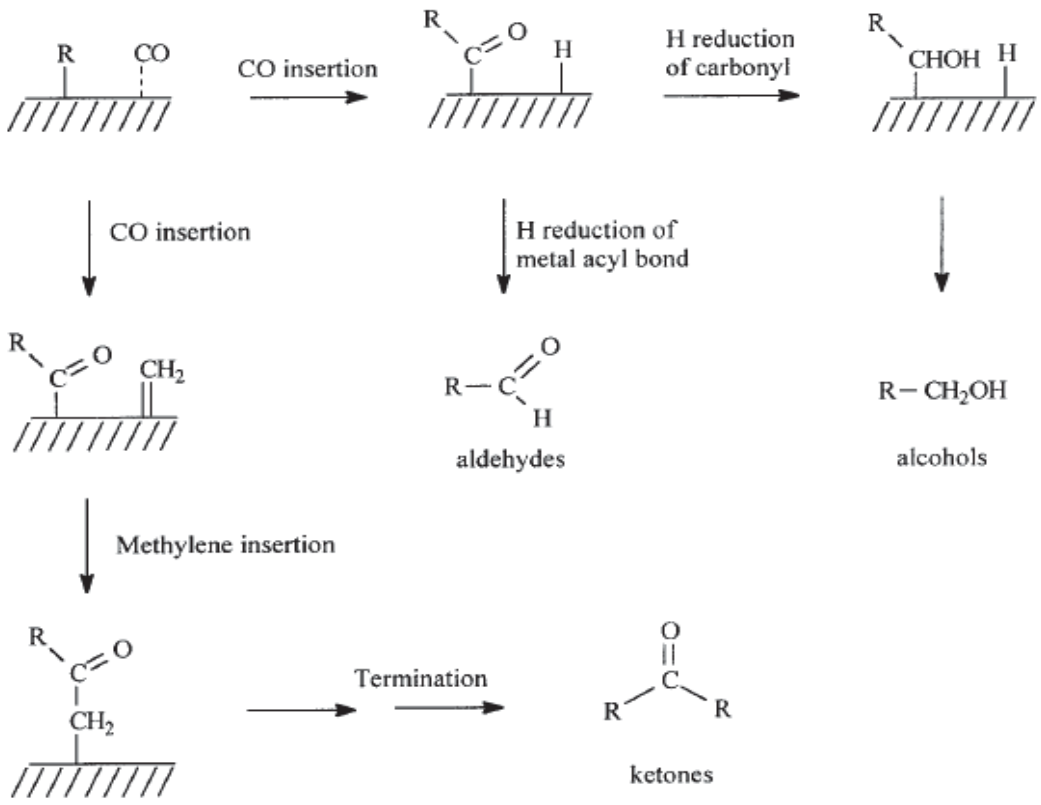

Figure 3.4 Possible mechanisms for the formation of oxygenates in the Fischer-Tropsch reaction [30]

Conventional refinery processes can be used for upgrading of Fischer-Tropsch liquid and wax products. A number of possible processes for FT products are wax hydrocracking, distillate hydrotreating, catalytic reforming, naphta hydrotreating, alkylation and isomerization [36, 37]. Fuels produced with the FT synthesis are of a high quality due to a very low aromaticity and zero sulfur content. The product stream consists of various fuel types: LPG, gasoline, diesel fuel, jet fuel. The definitions and conventions for the composition and names of the different fuel types are obtained from crude oil refinery processes and are given in Table 3.2.

Table 3.2 Conventions of fuel names and composition [28]

Name	Synonyms	Components
Fuel gas		C_1 - C_2
LPG		C_3 - C_4
Gasoline		C_5 - C_{12}
Naphtha		C_8-C_{12}
Kerosene	Jet fuel	C_{11}-C_{13}
Diesel	Fuel oil	C_{13}-C_{17}
Middle distillates	Light gas oil	C_{10}-C_{20}
Soft wax		C_{19} - C_{23}
Medium wax		C_{24} - C_{35}
Hard wax		C_{35+}

Modeling the product distribution from the Fischer-Tropsch synthesis is a challenging task, and an exact representation has proven difficult to establish [37]. The hydrocarbon product chain distribution in the Fischer-Tropsch synthesis was in part described by a chain polymerization kinetics model, the Anderson-Schulz-Flory (ASF) model [38]. This model was an ideal representation of the stepwise addition of one carbon atom to the growing chain, and the prediction of the hydrocarbon isomer distribution [39]. However, for all Fischer-Tropsch catalysts deviations from this ideal representation was observed. Bartholomew et al. [38] gave the mathematical presentation of the ASF distribution as follows:

$$\log(W_n/n) = n \log \alpha + \text{constant}$$

W_n is the mass fraction of the species with carbon number *(n)*. From the slope of the plot of log (W_n/n) against n, the value of α was obtained. It was usually found that over the carbon number range from 3 to about 12 the plots were linear and therefore over this range α was constant. However, in practice, “ideal” molecular weight distribution was never observed [37]. Figure 3.5 shows hydrocarbon selectivity in the FTS modeled by the Anderson-Schulz-Flory distribution.

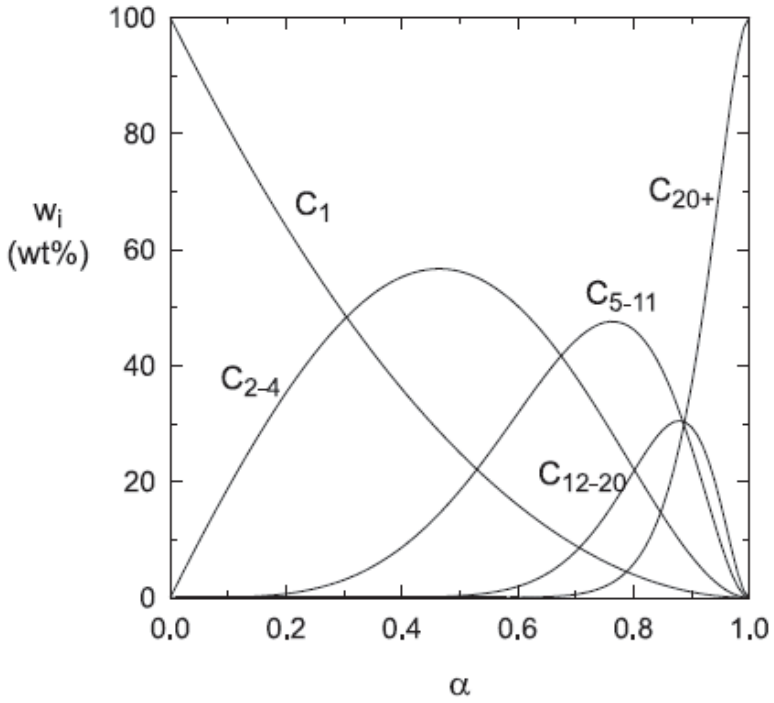

Figure 3.5 Hydrocarbon selectivity modeled by the Anderson-Schulz-Flory distribution [28]

CHAPTER 4

EXPERIMENTS

This chapter describes the experimental systems and procedures used in this study. It is divided into three parts consisting of catalyst preparation, catalyst characterization and catalyst evaluation. The first part explains catalyst preparation by flame spray pyrolysis and impregnation techniques. The second part shows the details of characterization techniques containing X-ray diffraction (XRD), N_2 physisorption, transmission electron microscopy (TEM), temperature programmed reduction (TPR), H_2 chemisorption, and X-ray photoelectron spectroscopy (XPS). Finally, a detailed procedure for catalyst evaluation in Fischer-Tropsch synthesis (FTS) is explained.

4.1 Catalyst Preparation

The chemicals used in the catalyst preparation are all analytical grades as listed in Table 4.1. It is noted that specification of these chemicals about physical properties is exhibited later in Appendix A.

Table 4.1 The details of chemicals used in the catalyst preparation

Chemicals	Formula	Grade	Manufacture
Aluminium-tri-sec-butoxide	$Al(OCH(CH_3)C_2H_5)_3$	97 wt% in butanol	Sigma-Aldrich Cheme GmbH, Germany
Cobalt naphthenate	$Co(C_{11}H_{10}O_2)_2$	10 wt% in mineral spirits	Fluka
Cobalt (II) nitrate hexahydrate	$Co(NO_3)_2{\cdot}6H_2O$	99.999%	Sigma-Aldrich Cheme GmbH, Germany
Ruthenium (III) nitrosyl nitrate solution	$Ru(NO)(NO_3)_x(OH)_y$, x+y=3	1.5 wt% in nitric acid	Sigma-Aldrich Cheme GmbH, Germany
Xylene	$C_6H_4(CH_3)_2$	≥ 99.8%	Merck KGaA, Germany

4.1.1 Preparation by Flame Spray Pyrolysis

The FSP technique was used for preparation of support and catalysts. Aluminium-tri-sec-butoxide (97 wt% in butanol) and cobalt naphthenate (10 wt% in mineral spirits) were used as precursor, which was diluted with xylene to a 0.5 M solution. The mixed precusor was injected through the center capillary of the FSP nozzle by a syringe pump at 5 ml/min. Oxygen was fed at 5 l/min through the surrounding annulus dispersing the solution into droplets. The pressure drop at the nozzle was held constant at 1.5 bar by adjusting the annulus gap width. A supporting premixed CH_4/O_2 surrounded by the dispersion oxygen annulus ignited and stabilized the spray flame. A sinter metal ring surrounding the CH_4/O_2 flame was supplied by additional 5 l/min O_2-sheath. The equipment of FSP is shown in Figure 4.1.

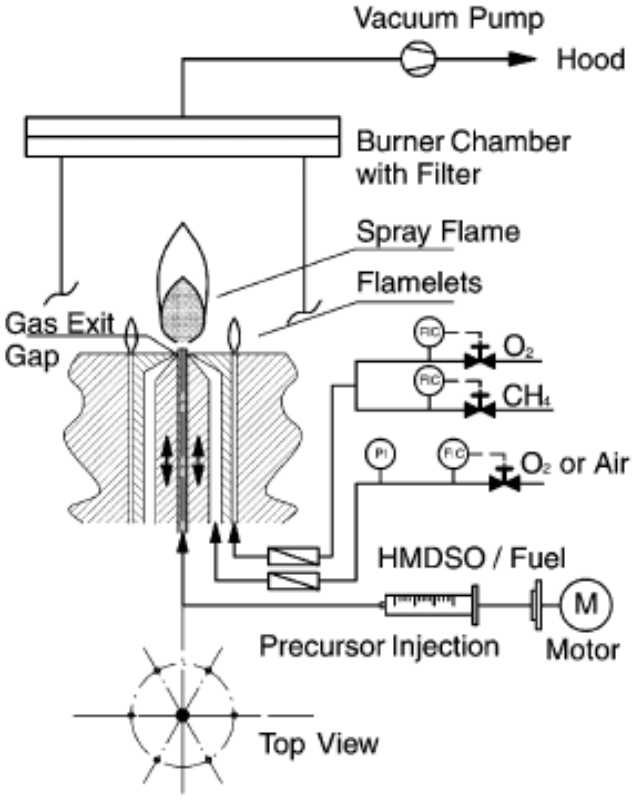

Figure 4.1 Experimental set-up scheme of flame spray pyrolysis [18]

4.1.2 Metal Loading by Wet Impregnation

The support, Al_2O_3 or Co-incorporated Al_2O_3, was impregnated by the metal stock solution (cobalt nitrate and/or ruthenium (III) nitrosyl nitrate). The support and metal solution were mixed in a flask. The mixed material was stirred at least 6 h at 70 ^{o}C. Subsequently, the sample was dried at 110 °C overnight. Finally, the catalyst was calcined in 30 ml/min of airflow at 500 °C for 4 h.

To accommodate for discussion, the catalysts used in this research are symbolically assigned as shown in Table 4.2.

Table 4.2 The symbol of the catalysts prepared using the different methods

Catalysts	Symbol
Al_2O_3 prepared by FSP	Al_2O_3
10 wt% Co impregnated on Al_2O_3 prepared by FSP	10Co/A
20 wt% Co impregnated on Al_2O_3 prepared by FSP	20Co/A
10 wt% Co impregnated on 10 wt% Co incorporated with Al_2O_3 by FSP	10Co/10Co-A
10 wt% Co incorporated with Al_2O_3 by FSP	10Co-A
20 wt% Co incorporated with Al_2O_3 by FSP	20Co-A
0.1 wt% Ru impregnated on 20 wt% Co incorporated with Al_2O_3 by FSP	0.5Ru/20Co-A
0.5 wt% Ru-10 wt% Co co-impregnated on 10 wt% Co incorporated with Al_2O_3 by FSP	10Co-0.5Ru /10Co-A
0.5 wt% Ru-20 wt% Co co-impregnated on Al_2O_3 prepared by FSP	20Co-0.5Ru/A
20 wt% Co impregnated on 0.1 wt% Ru incorporated with Al_2O_3 by FSP	20Co/0.5Ru-A
10 wt% Co impregnated on 10 wt% Co-0.1 wt% Ru incorporated with Al_2O_3 by FSP	10Co/10Co-0.5Ru-A
20 wt% Co-0.5 wt% Ru incorporated with Al_2O_3 by FSP	20Co-0.5Ru-A

4.2 Catalyst Characterization

4.2.1 X-ray Diffraction (XRD)

The X-ray diffraction (XRD) patterns of powder were obtained using an X-ray diffractometer BRUKER D8 ADVANCE connected with a computer with Diffract Plus TROPAS 4.2 programmed for fully control of the XRD analyzer. The experiments were carried out using Ni-filtered CuKα radiation. Scans were performed over the 2θ ranges from 20° to 80°. The crystallite size was estimated from line broadening according to the Scherrer equation. This instrument has been located at National Nanotechnology Center (NANOTEC), National Science and Technology Development Agency (NSTDA).

4.2.2 N_2 Physisorption

The BET surface areas for the multipoint method were measured by N_2 physisorption using BEL SORP mini II. The catalysts were firstly pretreated in 50 ml/min of helium gas flow at 150 °C for 3 h. Sample pretreatment system was used to remove water bound to the particle surface from air moisture. After cooled down to the ambient temperature, the weight of dried catalyst was collected. Sample cell was installed to the adsorption part. The requisite data were input to the software before the measurement. The sample cell was dipped in the dewar containing liquid nitrogen. The volume of N_2 was measured at -196 °C using the different N_2 partial pressure and then the adsorption-desorption isotherm was plotted.

4.2.3 Transmission Electron Microscopy (TEM)

The sizes and shapes of the samples were observed by a transmission electron microscope (JEOL, JEM-2010) operated at 200 kV. This instrument has been located at National Metal and Materials Technology Center, National Science and Technology Development Agency (NSTDA), Thailand. The sample was dispersed in ethanol to obtain the uniform dispersion of sample. A drop of liquid was deposited onto a copper mesh sample grid that supported a holey carbon support film. The grid was resting on a filter paper and was allowed to dry for several minutes before being moved. The scans were done many times in different areas as much as possible until the good representative image for all areas was obtained.

4.2.4 Temperature Programmed Reduction (TPR)

Temperature programmed reduction was used to determine the reducibility of catalysts. The hydrogen consumption was measured by using a Micrometritics Pulse Chemisorb 2750 instrument at Center of Excellence on Catalysis and Catalytic Reaction, Department of Chemical Engineering, Chulalongkorn University.

10% H_2 in Ar and N_2 in ultra high purity grade were used as a probe molecule gas and a carrier gas, respectively. 0.1 g of a catalyst sample was placed in a quartz tubular reactor. Under N_2 atmosphere at a flow rate of 25 ml/min, the catalyst sample was heated up to 250 °C at a heating rate of 10 °C/min and held for 1 h at this temperature in order to eliminate the adsorbed water. After the pretreatment, the system was cooled down to room temperature. The reduction step was performed under 10% H_2 in Ar flow of 25 ml/min from room temperature to 800 °C at a heating rate of 10 °C/min. It was noted that during the reduction step the water produced in this process was trapped by the liquid nitrogen. It was remarked that same samples were reduced by H_2 at 350 °C for 2 h before the reduction step.

4.2.5 Hydrogen Chemisorption

H_2 chemisorption was used to determine a number of cobalt metal atoms on the catalyst surface and overall cobalt dispersion. The total hydrogen consumption was calculated from the number of injection of a known volume. H_2 chemisorption was carried out using a Micrometritics Pulse Chemisorb 2750 instrument at Center of Excellence on Catalysis and Catalytic Reaction, Department of Chemical Engineering, Chulalongkorn University.

N_2 and H_2 were used as a carrier gas and a reducing/adsorbent gas, respectively. 0.1 g of a catalyst sample was placed in a quartz tubular reactor. Under H_2 atmosphere at a flow rate of 50 ml/min, the catalyst sample was heated up to 350 °C at a heating rate of 10 °C/min and held for 2 h at this temperature in order to reduce catalysts. After the reduction, the system was cooled down to room temperature by N_2 at a flow rate of 30 ml/min. Then, the catalyst sample was heated up to 100 °C at a heating rate of 10 °C/min by N_2. At this temperature, the catalyst sample was ready to be measure the metal active sites. 100 μl of the purity H_2 gas was

injected into the injection port to adsorb on the metal surface of the catalyst sample. Injection of H_2 was continuously repeated until saturation. This situation was occurred when an obtained chromatogram area of any injection, after adsorption of the H_2 pulse in the first injection had proceeded, was kept nearly constant compared with that of the former injection.

4.2.6 X-ray photoelectron spectroscopy (XPS)

The XPS analysis was performed originally using an AMICUS spectrometer equipped with a Mg K_α X-ray radiation at Center of Excellence on Catalysis and Catalytic Reaction, Department of Chemical Engineering, Chulalongkorn University. For a typical analysis, the source was operated at voltage of 15 kV and current of 12 mA. The pressure in the analysis chamber was less than 10^{-5} Pa.

For each and every element, there was a characteristic binding energy associated with each core atomic orbital i.e. each element gave rise to a characteristic set of peaks in the photoelectron spectrum at kinetic energies determined by the photon energy and the respective binding energies. The presence of peaks at particular energies therefore indicated the presence of a specific element in the sample under study - furthermore, the intensity of the peaks was related to the concentration of the element within the sampled region. Thus, the technique provided a quantitative analysis of the surface composition and was sometimes known by the alternative acronym, ESCA (Electron Spectroscopy for Chemical Analysis). The most commonly employed x-ray sources were those giving rise to:

Mg K_a radiation : h_n = 1253.6 eV Al K_a radiation : h_n = 1486.6 eV

The emitted photoelectrons will therefore have kinetic energies in the range of ca. 0-1480 eV. Since such electrons had very short IMFPs in solids, the technique was necessarily surface sensitive.

4.3 Catalyst Evaluation

The catalytic activity and product selectivity of all samples were tested by Fischer-Tropsch synthesis in a fixed-bed reactor at 220 °C under atmospheric pressure. The gases used in catalytic activity and product selectivity test are listed in Table 4.3. They were all supplied by Thai Industrial Gas Limited.

Table 4.3 The details of gases used in the catalyst activity test

Gases	Formula	Grade
Carbonmonoxide	CO	30% in H_2
Helium	He	Ultra high purity
Hydrogen	H_2	Ultra high purity

Figure 4.2 shows the flow diagram of the system for testing the catalytic activity product selectivity. The apparatus consisted of a fixed-bed reactor, an electrical furnace, an automation temperature controller, a gas controlling system, FID and TCD gas chromatographs.

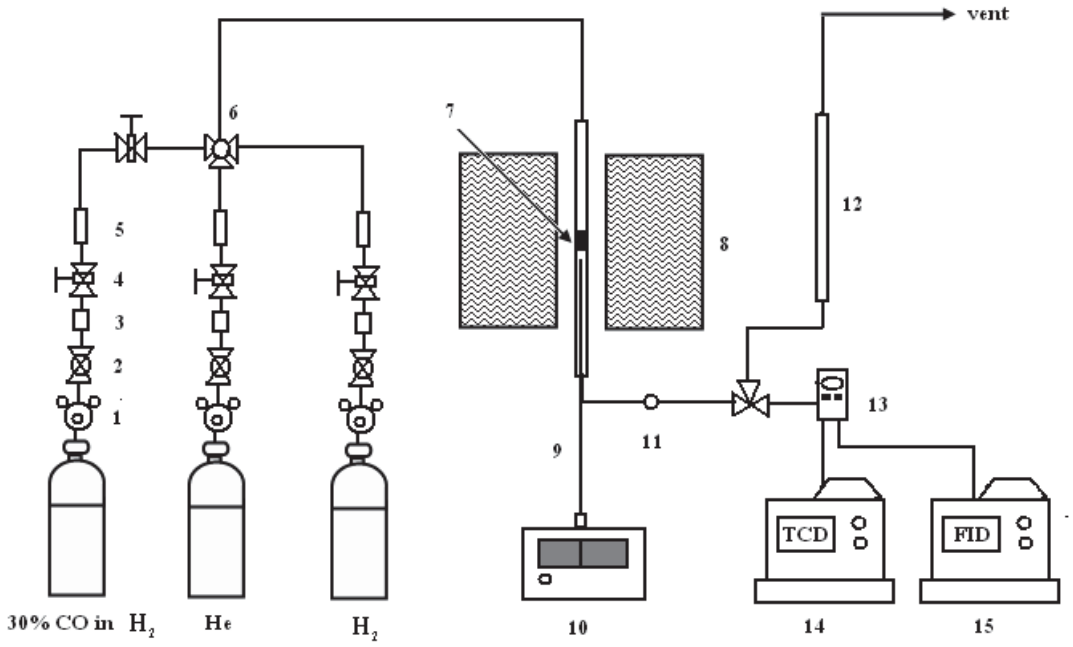

1. Pressure Regulator
2. On-Off Value
3. Gas Filter
4. Metering Valve
5. Check Valve
6. 3-way Valve
7. Catalyst Bed
8. Furnace
9. Thermocouple
10. Temperature Controller
11. Heating Tape
12. Bubble Flow Meter
13. Sampling Valve
14. GC-TCD
15. GC-FID

Figure 4.2 Schematic diagram of the reaction line for testing the FTS analyzed by GC-TCD and GC-FID equipped with Porapak Q and DB-1 column, respectively [40]

Catalytic activity measurements were carried out in a fixed bed stainless steel tubular reactor (0.95 cm. inside diameter). The catalyst sample was placed between two quartz wool layers. The gas flows were adjusted by the metering valves. The electrical furnace was used to supply heat to the reactor. The reactor could be operated from room temperature up to 800 °C at the maximum voltage of 220 V.

Reactor temperature was measured at the bottom of the catalyst bed in the reactor by automation temperature controller.

Reaction products were analyzed online by two Shimadzu GC-14B gas chromatographs with TCD (thermal conductivity detector) and FID (flame ionization detector). The operating conditions for each instrument are shown in the Tables 4.4 and 4.5, respectively.

Table 4.4 The operating conditions of TCD gas chromatographs for the catalytic activity test

Gas chromatograph	**Shimadzu GC-14B**
Detector	TCD
Column	Porapak Q
Carrier gas	He (UHP)
Carrier gas flow	30 ml/min
Injector temperature	150 °C
Detector temperature	150 °C
Column temperature	40 °C
Analysis gas	CO and CH_4

0.2 ml of catalyst sample was packed in a fixed-bed reactor placed in the furnace. Prior to the catalytic activity test, the temperature was raised to 350 °C in helium flow rate of 30 ml/min with a heating rate of 10 °C/min and the catalyst was reduced by hydrogen with flow rate of 30 ml/min at 350 °C for 2 h. After the reduction, the reactor was cooled to 220 °C in helium flow under atmospheric pressure. The reactant feed consisted of H_2 and CO at H_2/CO ratio of 2.33. The total volumetric flow rate was 30 ml/min. The reactant was switched at this temperature and the product samples were collected at 5, 90 and 180 min. The composition of hydrocarbons in the product was analyzed by two on-line gas chromatographs (GC) connecting with FID and TCD detectors.

Table 4.5 The operating conditions of FID gas chromatograph for the catalytic activity test

Gas chromatograph	**Shimadzu GC-14B**
Detector	FID
Column	DB-1
Carrier gas	N_2 (UHP)
Split/Splitless	Split
Purge flow rate	10 ml/min
Carrier pressure	150 kPa
Make up pressure	50 kPa
Injector temperature	200 °C
Detector temperature	200 °C
Column temperature	40 °C (held 10 min) and then raised at 5 °C/min to 250 °C (held 10 min)
Analysis gas	Hydrocarbons

CHAPTER 5

RESULTS AND DISCUSSION

The main topic of this research involves the use of Co supported on alumina catalysts in the Fischer-Tropsch synthesis. The results and discussion in this chapter are divided into three sections. In the first section, the physical and chemical properties of Co based catalysts are pronounced. The catalytic performance for the Fischer-Tropsch synthesis is evaluated in the two later sections. The effect of Co content between impregnation and incorporation was first studied and then the effect of ruthenium promoter was investigated.

5.1 The Physical and Chemical Properties of Cobalt Based Catalysts

In this part, the catalytic properties were characterized by various methods. The phase identification was determined by the X-ray diffraction technique. The morphology and particle characteristics were focused by transmission electron microscopy (TEM). The N_2 physisorption showed the BET surface area, the mean pore diameter, the pore volume and the particle diameter. The adsorption/desorption isotherms and the pore size distribution, which were also obtained by the N_2 physisorption, indicated the pore characteristics of the catalysts. The temperature programmed reduction (TPR) exhibited reduction behavior and reducibility of the catalysts. The metallic cobalt sites, cobalt dispersion as well as particle sizes of metallic cobalt were evaluated by H_2 chemisorption technique. The surface composition of the catalysts was determined by X-ray photoelectron spectroscopy (XPS).

5.1.1 The Phase Analysis by X-ray Diffraction (XRD)

The X-ray diffraction pattern of Al_2O_3 support prepared by FSP is shown in Figure 5.1. The Al_2O_3 support contained three mixed phases of chi phase, gamma phase and alpha phase. The XRD peaks at 43° were evident for the chi phase whereas those at 32°, 37°, 39°, 46°, 61° and 66° were assigned as the gamma phase and the peaks at 34°and 57° were evident to identify the alpha phase [41]. The Co incorporated with Al_2O_3 by FSP shows two mixed phases between gamma and chi phase as shown in Figure 5.2. This indicated that adding of Co during the FSP process can inhibit phase transformation of gamma to alpha phase. The other peaks were assigned to the spinel phases of Co_3O_4 or the different crystal phase of Co_3O_4-Al_2O_3 interaction species including cobalt aluminate ($CoAl_2O_4$). However, the pattern of peak intensities of the cubic spinel phase of Co_3O_4 and $CoAl_2O_4$ was rather similar [12]. It was difficult to establish the chemical and structural phase for those catalysts based only on the XRD characteristics. Fortunately, this problem can be resolved by the following XPS technique as discussed later. The addition of Ru on the Co-based catalysts was invisible as shown in Figures 5.3 and 5.4 due to very small content of added Ru or more importantly its high dispersion [4].

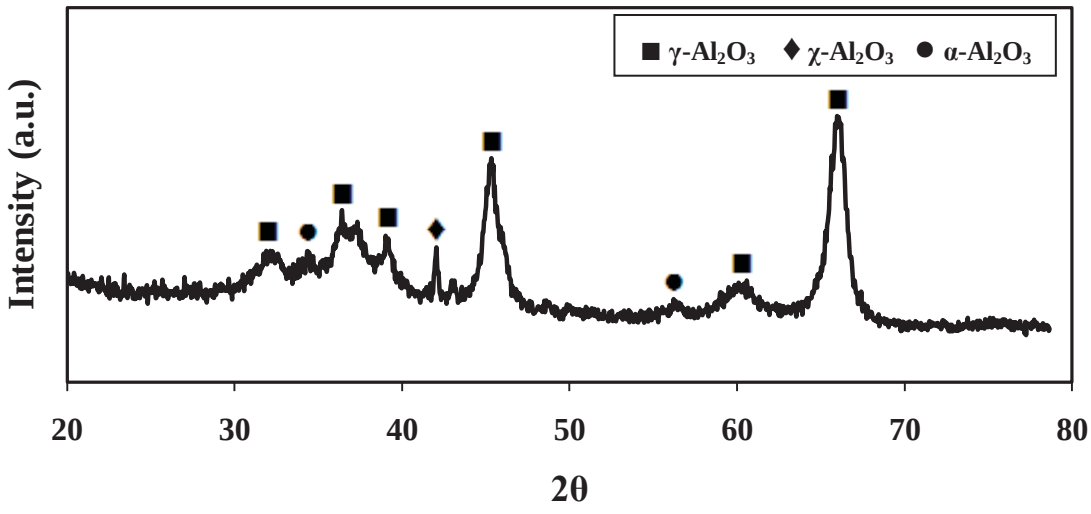

Figure 5.1 XRD patterns of the Al_2O_3 support by FSP

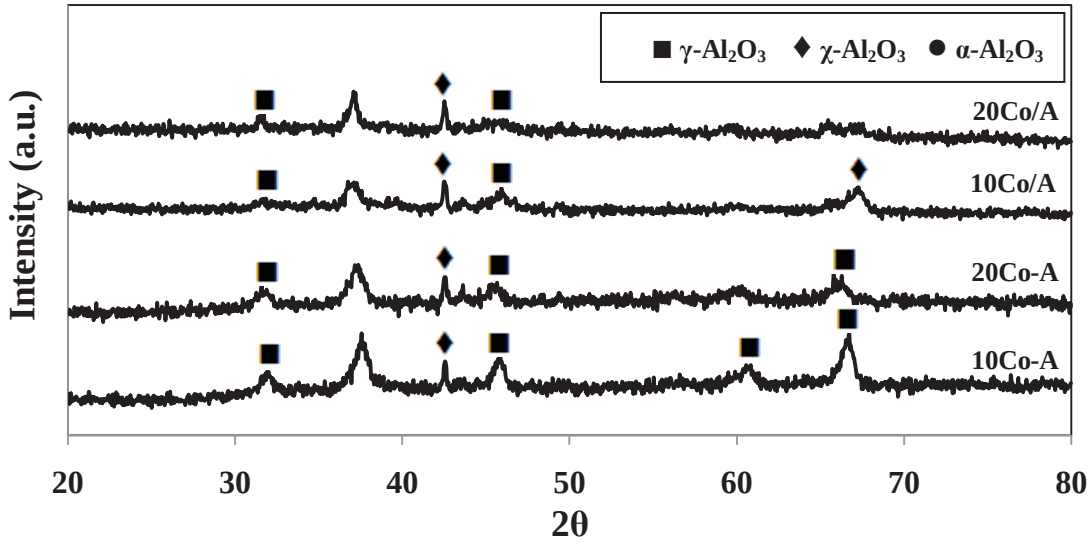

Figure 5.2 XRD patterns of the Co based catalysts prepared by FSP

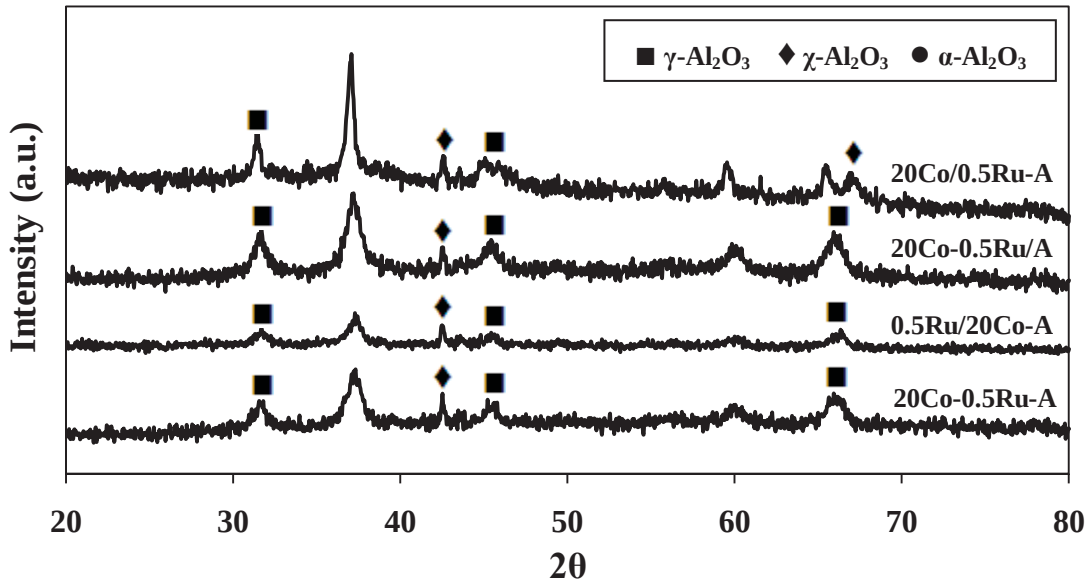

Figure 5.3 XRD patterns of the 20Co/A catalysts with various Ru addition techniques

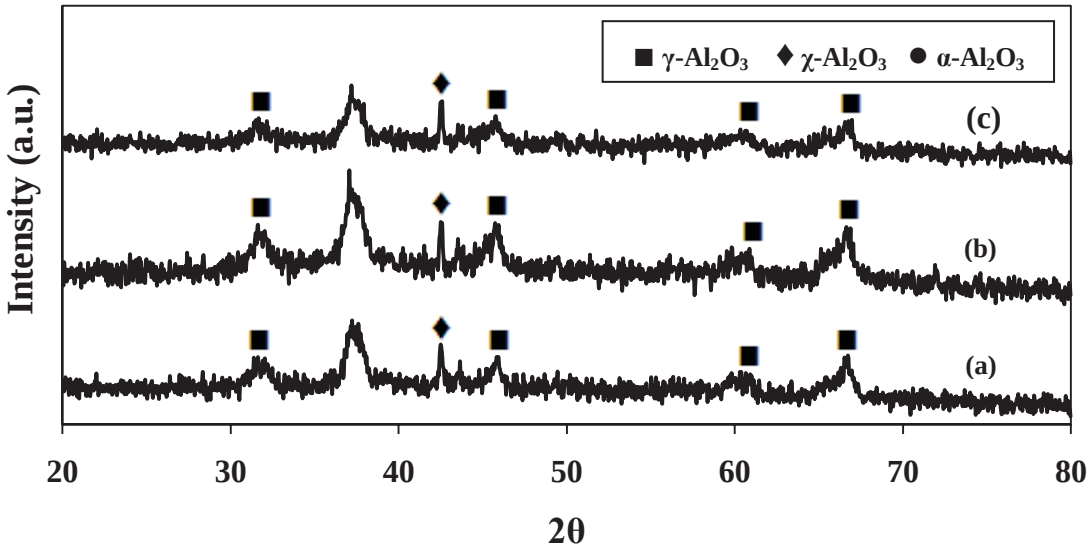

Figure 5.4 XRD patterns of the 10Co/10Co-A catalysts with various Ru addition techniques: (a) 10Co/10Co-A (b) 10Co/10Co-0.5Ru-A and (c) 10Co-0.5Ru/10Co-A

5.1.2 Transmission Electron Microscopy

In order to determine the particle morphology and the particle size distribution, a powerful technique such as TEM was applied to samples. TEM micrographs of Co catalysts are shown in Figures 5.5-5.9. The particle sizes of all catalysts were in range of 15-19 nm. The shape of particles was rather spherical and non-hollow. The particle sizes of catalysts prepared by FSP were varied because it was difficult to control particle formation during the flame spray process. The particles in FSP were produced as a result of the competition between droplet vaporization and reaction inside the droplet. When the droplet vaporization was dominant, the vaporized precursors reacted in gas phase and particle growth occurred by collision and coalescence. On the contrary, when the intradroplet reaction was dominant, the precursor droplet underwent hydrolysis and/or oxidation within the confines of the sprayed liquid droplet and one droplet produces one particle [26]. The overlap between particles indicating collision and coalescence of some particles during FSP was also found. Some large particles were clearly observed when 20 wt% Co was impregnated on the Al_2O_3 as shown in Figure 5.5. These particles were

possible to be cubic spinel phase of Co_3O_4 or $CoAl_2O_4$ consistent with appearance of the peak in the XRD result. More overlap between particles was clearly observed for the catalyst prepared by impregnation. Figure 5.9 shows that the particles obtained by addition of Co and Ru incorporated with Al_2O_3 by FSP were rather similar to those of 20Co-A. It was indicated that Co and Ru, which were formed during FSP, were well dispersed on the Al_2O_3 support. Figure 5.8 shows TEM image of the 20Co/0.5Ru-A catalyst. This was rather similar to 20Co/A. This indicated addition of Ru did not disturb the formation of Al_2O_3 support.

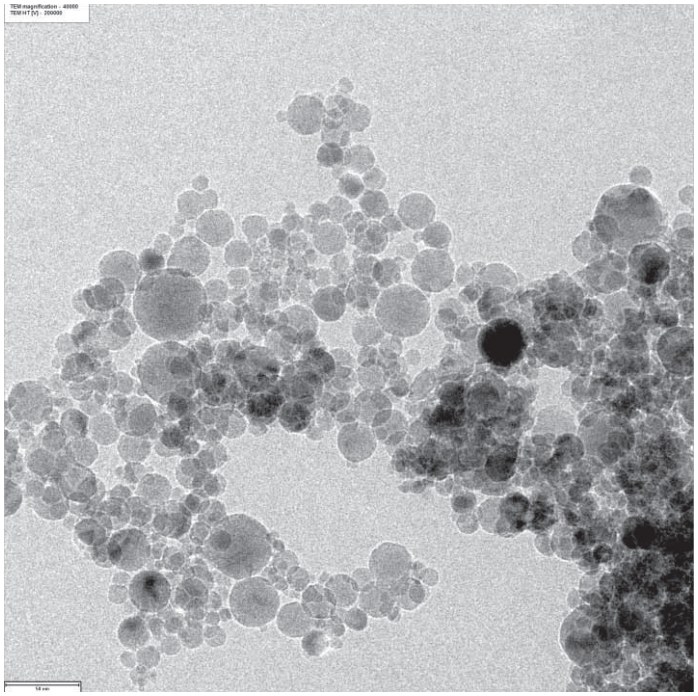

Figure 5.5 Transmission electron microscopy images of 20Co/A catalyst

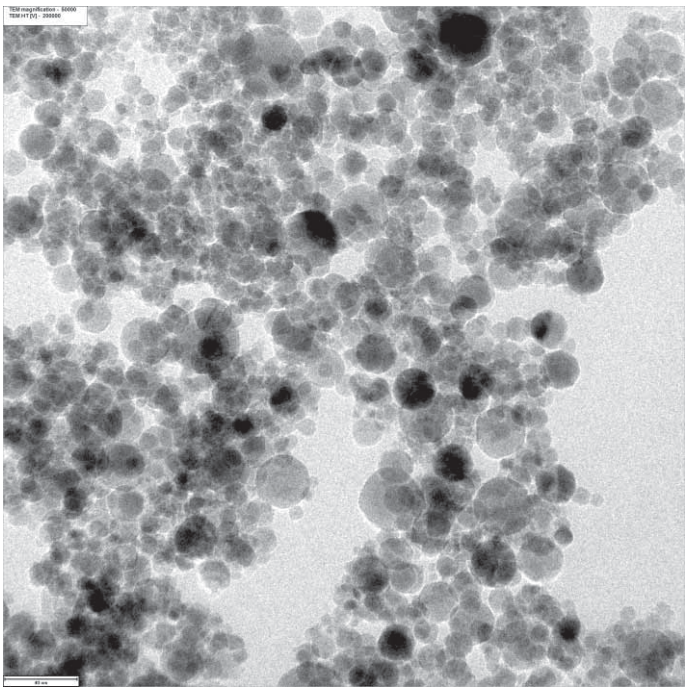

Figure 5.6 Transmission electron microscopy images of 20Co-A catalyst

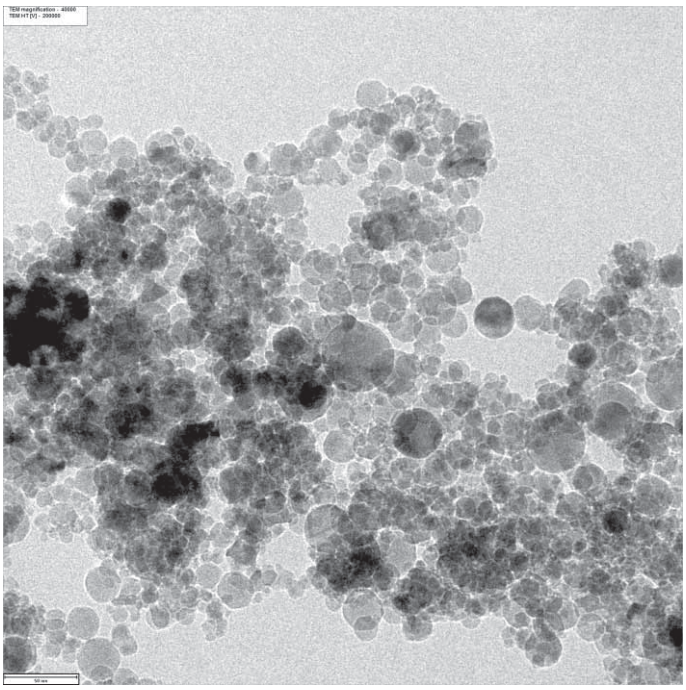

Figure 5.7 Transmission electron microscopy images of 10Co/10Co-A catalyst

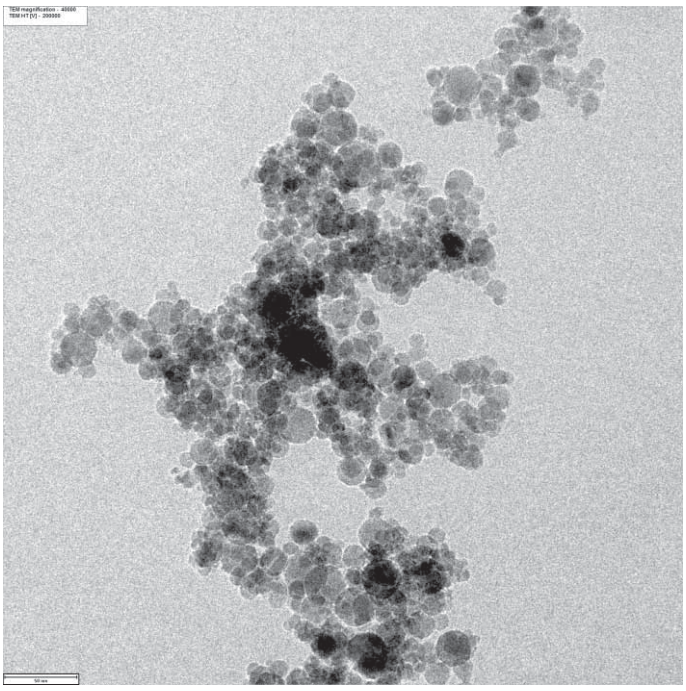

Figure 5.8 Transmission electron microscopy images of 20Co/0.5Ru-A catalyst

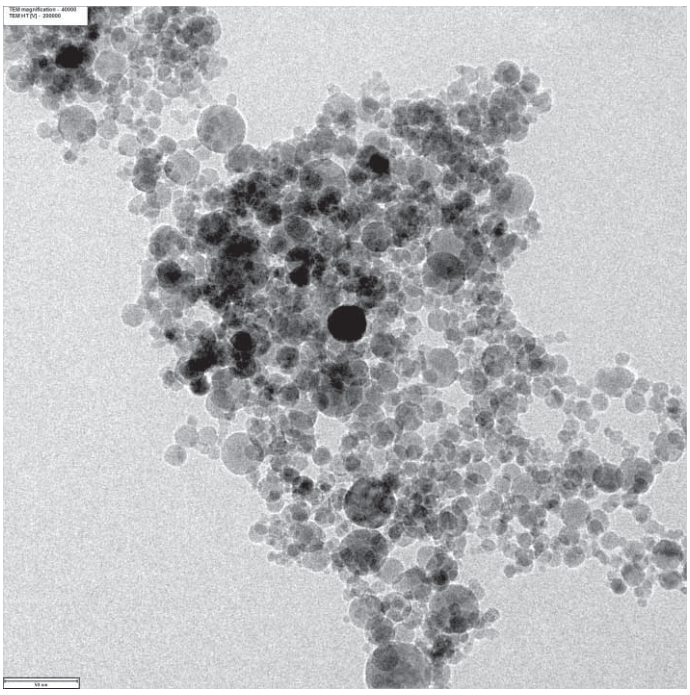

Figure 5.9 Transmission electron microscopy images of 20Co-0.5Ru-A catalyst

5.1.3 The BET Surface Area and Pore Characteristics

The BET surface area, the mean pore diameter, the particle diameter and the pore volume of cobalt based catalysts were determined by adsorption and condensation of N_2 at liquid N_2 temperature using static vacuum procedure. These results are given in Table 5.1. The BET surface area, the mean pore diameter and the pore volume of the 10Co-A were similar to the Al_2O_3 support. This indicated that at low Co loading incorporated during FSP did not disturb the formation of Al_2O_3 particles resulting in the same pore characteristics of catalyst. On the other hand, Co loaded by impregnation decreased apparently the BET surface area, the mean pore diameter and the pore volume of the catalysts. It was noted that both the mean pore diameter and the pore volume decreased with increasing percentage of cobalt loading. This was due to blocking pores of the cobalt consistent with the literatures [12]. However, as compared with the 20Co/A, the BET surface area was increased when cobalt and ruthenium were co-impregnated on the Al_2O_3. This was possible that ruthenium could promote dispersion of Co_3O_4 on the catalyst surface and provide smaller Co_3O_4 particle sizes. This result was consistent with the literatures [42, 43].

Figures 5.10-5.14 show the N_2 adsorption/desorption isotherms and the pore size distribution of Al_2O_3 support and Co based catalysts. All of isotherms showed hysteresis loop indicating the presence of closed or opened pores. They were associated with ink-bottle pores where entrance to the pore was narrower than the body [44]. This indicated the existence of the mesoporous structure within the catalyst [45] consistent with results of the mean pore diameter in Table 5.1. The isotherms of the 10Co-A, 20Co-A and Al_2O_3 support were the same pattern. It was confirmed that Co incorporated during FSP did not disturb the pore characteristics within the Al_2O_3 structure. It was noted that the patterns of the pore size distribution were randomly varying in both samples. It was implied that the sizes of pore mouth could not be easily control by the FSP process. But the addition of Co by impregnation gave narrow pore size distribution and the isotherms were also changed as shown in Figures 5.13 and 5.14. This was due to blocking pores of cobalt oxide particles.

Table 5.1 The BET surface area, the mean pore diameter, the particle diameter and the pore volume of Co based catalysts

Catalysts	BET surface area[a] (m^2/g)	Mean pore diameter[a] (nm)	Particle diameter[b] (nm)	Total Pore volume[a] (cm^3/g)
Al_2O_3	66	28.8	23.0	0.47
10Co/A	48	10.5	30.5	0.13
20Co/A	52	9.6	25.9	0.13
10Co/10Co-A	81	3.0	16.7	0.06
10Co-A	72	30.2	20.1	0.54
20Co-A	72	10.6	18.7	0.19
0.5Ru/20Co-A	71	3.4	18.9	0.05
10Co-0.5Ru/10Co-A	68	3.2	19.8	0.05
20Co-0.5Ru/A	63	3.2	21.3	0.04
20Co/0.5Ru-A	58	3.1	23.2	0.04
10Co/10Co-0.5Ru-A	64	3.1	21.0	0.05
20Co-0.5Ru-A	71	3.1	18.9	0.05

[a] Using N_2 physisorption at -196 °C: Error of measurement ± 5%

[b]Based on BET surface area Mean : Particle diameter (nm) = $6/(\text{density} \times S_{BET})$

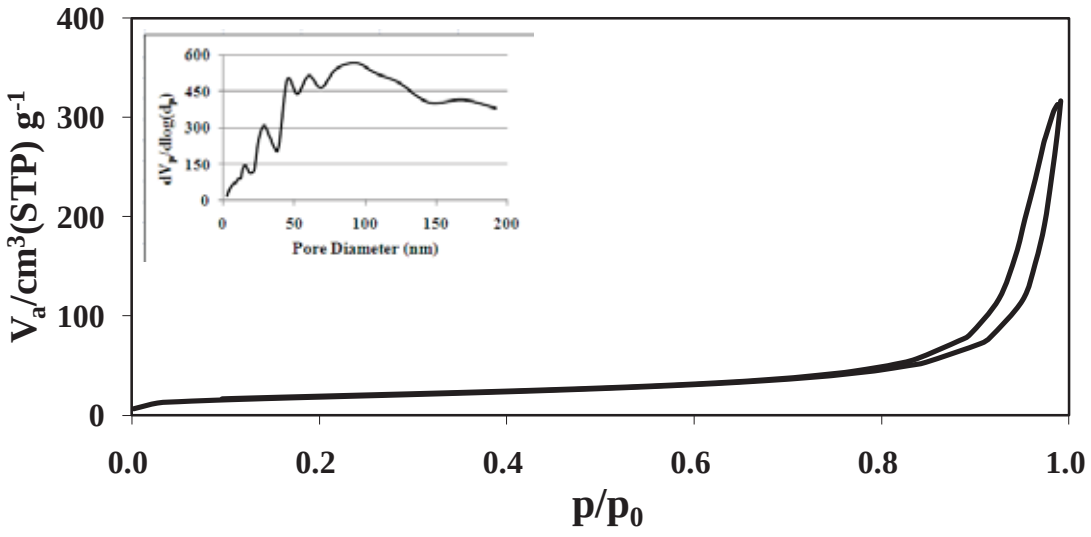

Figure 5.10 The N_2 adsorption/desorption isotherms and the pore size distribution of the Al_2O_3 support by FSP

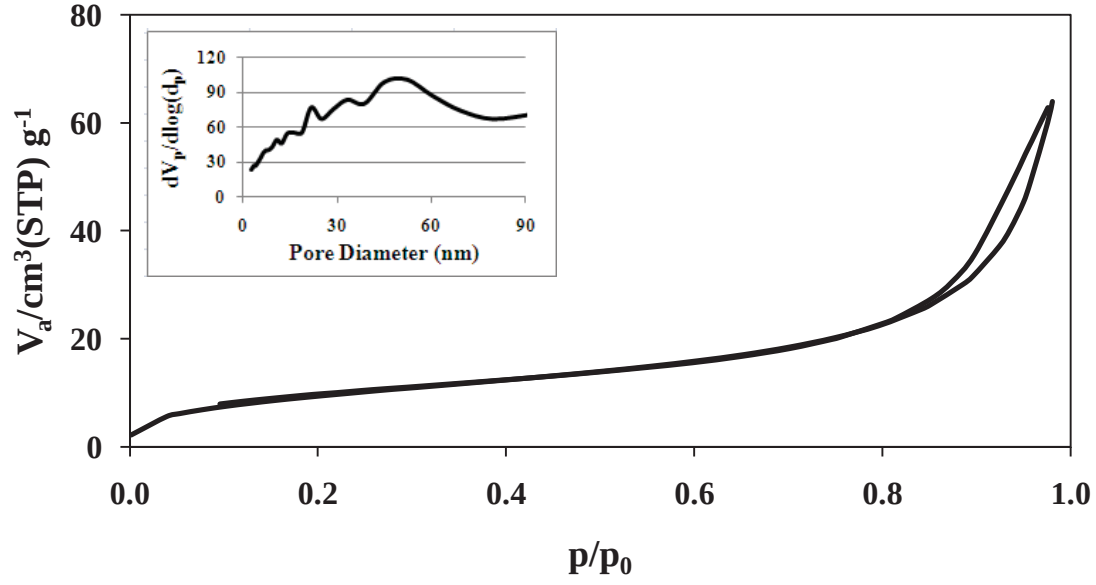

Figure 5.11 The N_2 adsorption/desorption isotherms and the pore size distribution of the 10Co-A

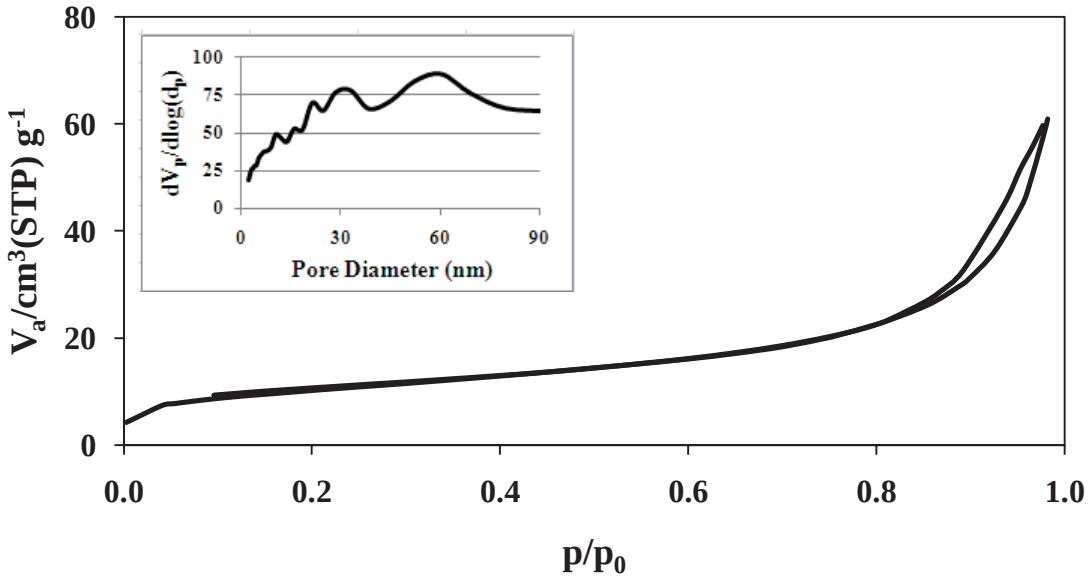

Figure 5.12 The N_2 adsorption/desorption isotherms and the pore size distribution of the 20Co-A

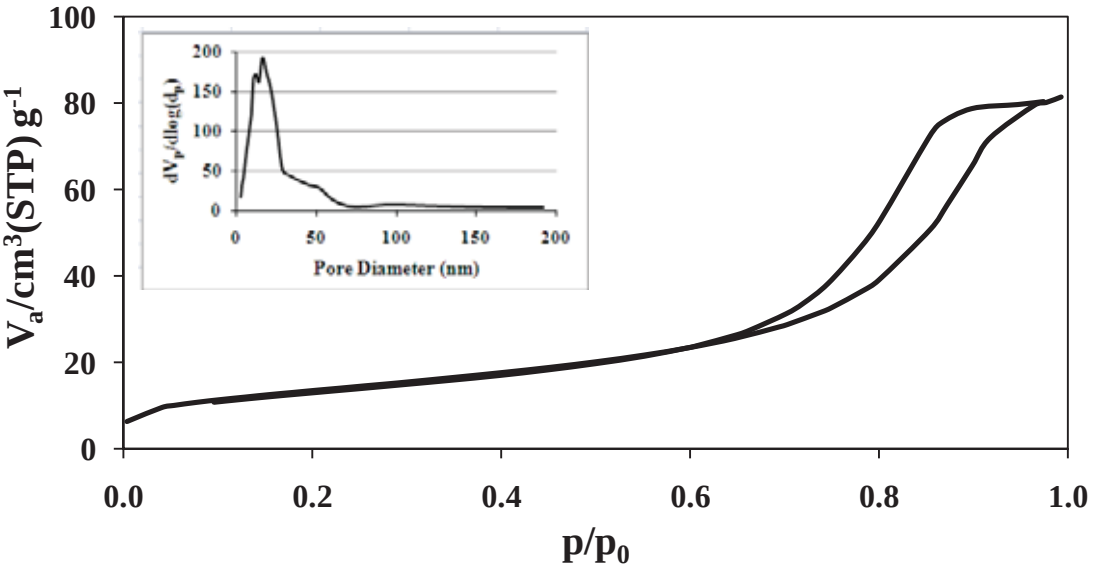

Figure 5.13 The N_2 adsorption/desorption isotherms and the pore size distribution of the 10Co/A

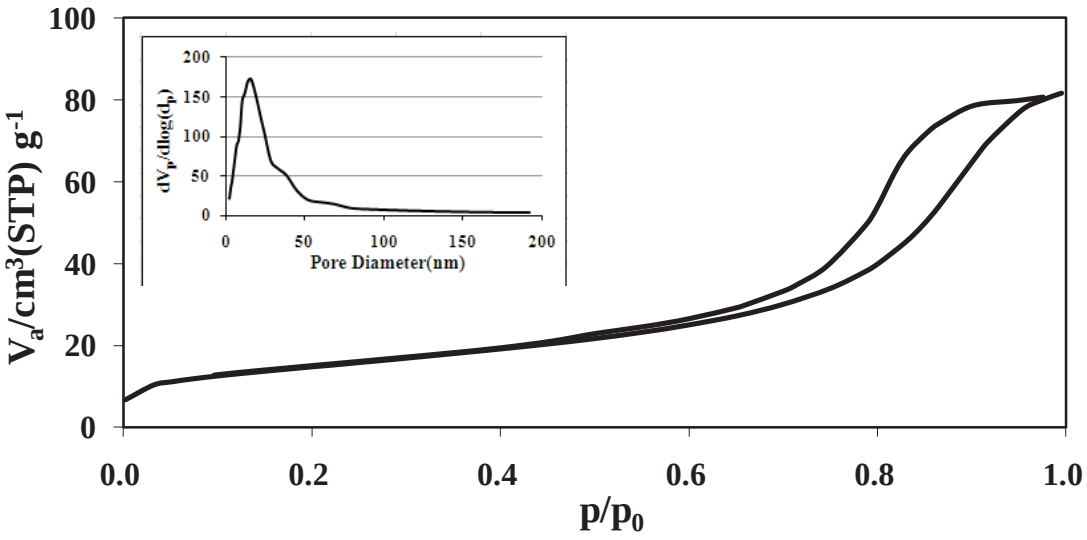

Figure 5.14 The N_2 adsorption/desorption isotherms and the pore size distribution of the 20Co/A

5.1.4 The Reduction Characteristics by TPR

Temperature programmed reduction (TPR) was performed in order to determine the reduction behaviors. TPR patterns are displayed in Figures 5.15 and 5.16. The solid line represented the reduction of the fresh catalysts and the dashed line gave the reduction pattern of the pre-reduced catalysts (The pre-reduction was occurred at 350 ºC for 2 h in hydrogen flow, which is the condition employed before the activity testing). All the fresh samples exhibited two main reduction peak region. In general, the first reduction peak appearing in the low temperature region (200-450 °C) was attributed to the overlap of two reduction steps of Co_3O_4 to CoO and CoO to metallic state of cobalt. The second reduction peak at high temperature (450-800 °C) can be assigned to the strong interaction between Co and Al_2O_3 support [46]. The temperature was not ramped high enough to observe the complete reduction of bulk $CoAl_2O_4$, which have been shown to occur about 1000 °C [12].

In Figure 5.15, the 20Co-A showed very slightly peak area compared with the other catalysts. The relatively high reduction temperature of 20Co-A was attributed to small cobalt size and the strong interaction with the Al_2O_3 support or the reduction peak of $CoAl_2O_4$ [47]. This indicated that the formation of $CoAl_2O_4$ occur during the FSP process. For the 20Co/A, the two-step reduction can be observed. It was found that the first reduction peak assigned to the overlap of two reduction step of Co_3O_4 to CoO and then to Co metal. The second reduction peak at high temperature can be assigned to Co_3O_4-Al_2O_3 interaction. The peak at the high temperature above 800 °C was disappeared. It was indicated that the $CoAl_2O_4$ cannot be formed during the calcination step.

Figure 5.16 shows the TPR patterns of Ru addition. The 0.5Ru/20Co-A and 20Co-0.5Ru-A showed the patterns similar to the 20Co-A. This indicated that Ru cannot be inhibit the formation of $CoAl_2O_4$ during the FSP process. The co-impregnation of Co and Ru on Al_2O_3 shifted the both peaks to the lower temperature. This was due to the interaction of cobalt oxide species with Al_2O_3 support was weaken. It was suggested that the addition of Ru promoted their reduction ability. The reducibility of all catalysts are shown in Table 5.2.

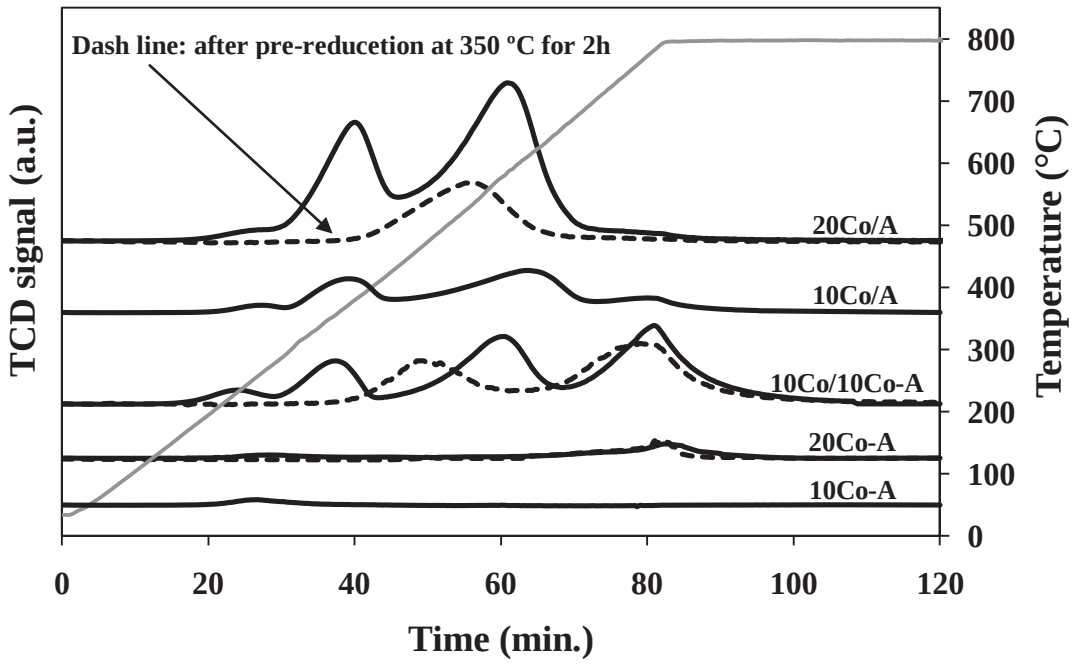

Figure 5.15 TPR patterns of Co based catalyst

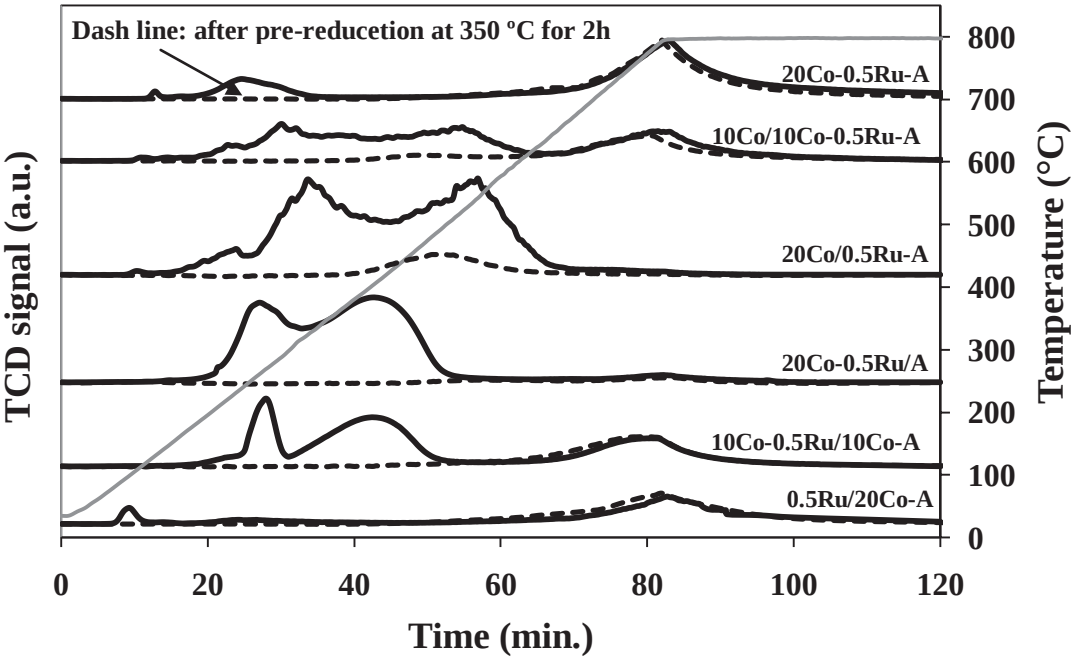

Figure 5.16 TPR patterns of Co based catalyst with various techniques of Ru addition

Table 5.2 The reducibility of all catalyts

Catalysts	Total Reducibility (%)[a]	Relative Reducibility (%)[b]
10Co/A	32.17	60.74
20Co/A	74.22	74.56
10Co/10Co-A	21.31	30.54
10Co-A	1.81	98.70
20Co-A	12.53	53.01
0.5Ru/20Co-A	15.21	27.66
10Co-0.5Ru/10Co-A	44.56	57.63
20Co-0.5Ru/A	91.19	94.52
20Co/0.5Ru-A	82.63	89.05
10Co/10Co-0.5Ru-A	53.39	64.71
20Co-0.5Ru-A	7.61	15.68

[a] The total reducibility (%) was defined [48]

$$\left[\frac{H_2\ consumption\ after\ calcinations - H_2\ consumption\ after\ pre\ reduction}{Theoretical\ H_2\ consumption\ for\ 20\ wt.\%Co\ catalysts}\right] \times 100$$

[b] The relative reducibility (%) was defined as follows:

$$\left[\frac{H_2\ consumption\ for\ calcined\ samples - H_2\ consumption\ for\ pre\ reduce\ samples}{H_2\ consumption\ for\ calcined\ samples}\right] \times 100$$

5.1.5 The Cobalt Metallic Sites by Hydrogen Chemisorption

The relative amounts of active cobalt metals on the catalyst samples were calculated from H_2 chemisorption experiments at 100 ℃ according to Bartholomew et al. [49]. It was known that only surface Co metal atoms were active for the Fischer-Tropsch synthesis not their oxides. The chemisorptions were calculated with the assumptions that the adsorption stoichiometry was H : CO = 1 and that Ru did not contribute to the amount of chemisorbed H_2.The results of H_2 chemisorption are shown in Table 5.3, provided the information on the number of cobalt active sites, Co dispersion and mean particle size of cobalt metal. For the Co incorporated with Al_2O_3 by FSP was not detected. This was due to the formation of $CoAl_2O_4$, which recognized as irreducible phase. The Co impregnated on Al_2O_3 exhibited higher cobalt active sites. Although the cobalt oxides on the Co impregnated on Al_2O_3 were large, all of them were easily reduced to metallic cobalt. The cobalt metallic size obtained by the reduction was smaller than the cobalt oxide size. It was implied that cobalt particles were easily reconstructed and well dispersed during the reduction step. The presence of Co and Ru incorporated with Al_2O_3 by FSP still no adsorption of H_2 on the catalyst surface. It suggested that Ru cannot inhibit the formation of $CoAl_2O_4$. The co-impregnation of Co and Ru on Al_2O_3 increased reducibility and metal dispersion. This was corresponding with the results of the Co impregnated on Ru incorporated with Al_2O_3 by FSP.

Table 5.3 The results obtained from H_2 chemisorption

Catalysts	The amount of adsorbed H_2[a]$\times 10^{-18}$ (molecule H_2/g cat)	Reducibility[b] (%)	Co dispersion[c] (%)	Metallic Co diameter[d]
10Co/A	2.51	32.17	7.6	12.6
20Co/A	7.32	74.22	9.7	9.9
10Co/10Co-A	2.12	21.31	9.7	9.9
10Co-A	n.d.	1.81	n.d.	n.d.
20Co-A	n.d.	12.53	n.d.	n.d.
0.5Ru/20Co-A	n.d.	15.21	n.d.	n.d.
10Co0.5Ru/10Co-A	7.28	44.56	16.0	6.0
20Co-0.5Ru/A	11.42	91.19	12.3	7.8
20Co/0.5Ru-A	12.93	82.63	15.3	6.3
10Co/10Co-0.5Ru-A	7.47	53.39	13.7	7.0
20Co-0.5Ru-A	n.d.	7.67	n.d.	n.d.

n.d. = not detectable

[a] Error of measurement = +/- 5%.

[b] The Reducibility (%) was defined

$$\left[\frac{\text{H}_2 \text{ consumption after calcinations} - \text{H}_2 \text{ consumption after pre reduction}}{\text{Theoretical H}_2 \text{ consumption for 20 wt.\%Co catalysts}}\right] \times 100$$

[c] Co dispersion (%) $= \left[\frac{\text{The amount of Co equivalent to H}_2 \text{ adsorption after reduction}}{\text{Total amount of Co active sites expected to exist after reduction}}\right] \times 100$

[d] Metallic Co diameter = 96/(% Cobalt dispersion) [50]

5.1.6 X-ray photoelectron spectroscopy (XPS) analysis

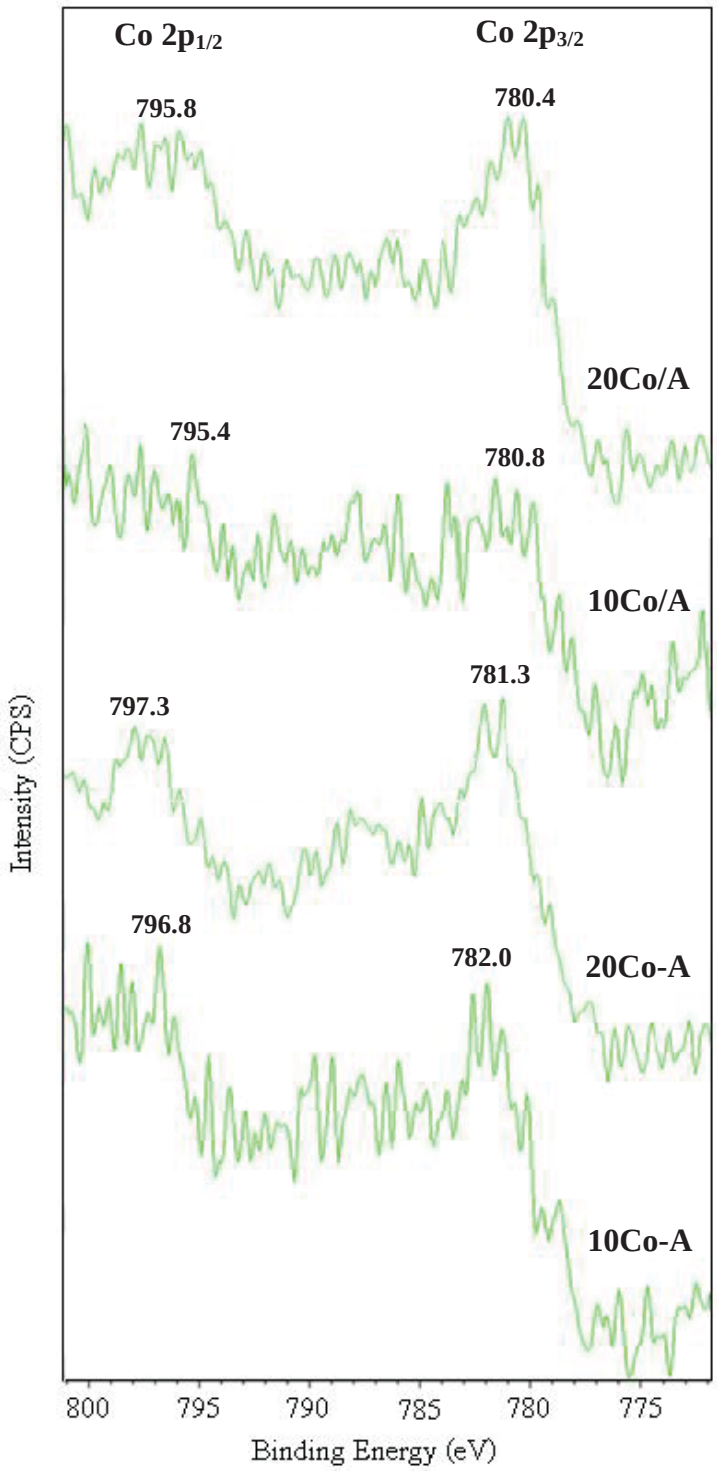

Figure 5.17 Co2p XPS spectra of Co-based catalysts

Table 5.4 The XPS Binding energy (BE) of cobalt based catalysts

Catalyst	XPS Binding energies* (eV)	
	Co $2p_{3/2}$	**Co $2p_{1/2}$**
10Co/A	780.8	795.4
20Co/A	780.4	795.8
10Co-A	782.0	796.8
20Co-A	781.3	797.3

* Error measurement ± 0.3 eV

The structure of the cobalt-based catalyst was investigated by surface sensitive XPS analysis. Figure 5.17 show the Co2p XPS spectra of Co-based catalysts. The analytical results on Co $2p_{3/2}$ and Co $2p_{1/2}$ are presented in Table 5.4, while the literature data of various Co-containing compounds are shown in Table 5.5. As shown in Table 5.4, the Co $2p_{3/2}$ component at 780.0 eV for 10Co/A and 20Co/A catalyst corresponded to Co_3O_4. The other component at 782.0 eV for 10Co-A and 20Co-A catalyst can be ascribed to $CoAl_2O_4$ phase. This indicated that FSP process can synthesize the $CoAl_2O_4$ compound. This was due to the $CoAl_2O_4$ can be formed by sintering the stoichiometric mixture of finely ground CoO and Al_2O_3 at high temperature (above 1000 ºC) [51, 52]. The flame could be maintained at temperatures high enough to complete thermal decompositions through intense oxidation.

Table 5.5 XPS data and characteristics of cobalt-containing reference materials [12]

Materials	Co $2p_{3/2}$ BE (eV)	Reliability
Co	778.1	±0.1
Co_3O_4	780.0	±0.7
$CoAl_2O_4$	781.9	±0.5

5.2 Fischer-Trospch Synthesis Activity over Cobalt Based Catalyst

Figure 5.18 show the reaction rate for FTS of Co-based catalyst. Table 5.6 shows the reaction rate and turn over frequency(TOF) for FTS of Co/Al_2O_3 catalyst at various times on stream. The 20Co/A show low reaction rate and TOF. The main product in this case was methane, which was not desired for the FTS. The 20Co-A showed lower activity than the 20Co/A. This was due to the $CoAl_2O_4$ form. The product selectivity of the 20Co-A preferred to the heavy hydrocarbons. The 10Co/10Co-A gave high reaction rate and TOF. It was remarked that the products in this case were light hydrocarbons and gasoline including heavy hydrocarbon. Figure 5.19 present the CH_4 selectivity of FTS Co/Al_2O_3 catalyst. Figure 5.20-5.22 show the product selectivity of Co/Al_2O_3 catalyst at various times on stream.

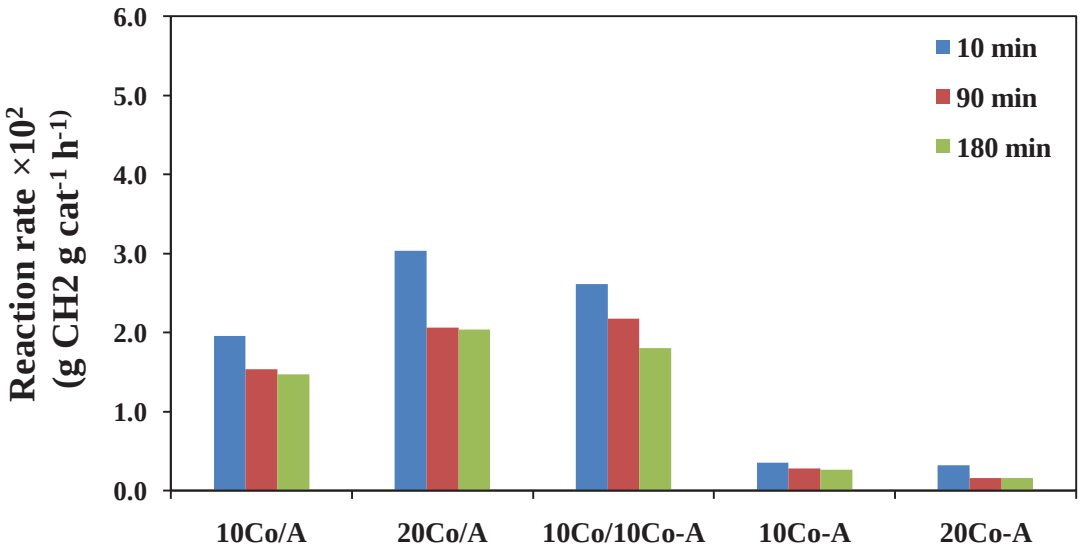

Figure 5.18 The reaction rate for FTS of Co-based catalyst

Table 5.6 The reaction rate and TOF for FTS of Co/Al_2O_3 catalyst

Catalysts	Time (min)	Reaction rate[a] $\times 10^2$ (g CH_2 $g_{cat}^{-1}h^{-1}$)	TOF[b] $\times 10^2$ (s^{-1})
10Co/A	10	1.96	2.07
	90	1.54	1.62
	180	1.47	1.56
20Co/A	10	2.37	0.46
	90	2.44	0.48
	180	2.56	0.50
10Co/10Co-A	10	3.27	2.09
	90	2.18	1.39
	180	1.80	1.15
10Co-A	10	0.36	n.d.
	90	0.28	n.d.
	180	0.27	n.d.
20Co-A	10	0.32	n.d.
	90	0.16	n.d.
	180	0.16	n.d.

[a] Rate of reaction (g CH_2 g_{cat}^{-1} h^{-1}) = $\frac{\text{CO conv.} \times \text{flow rate of CO in feed} \times \text{MW of } CH_2}{\text{Catalyst weight}}$

[b] TOF (s^{-1}) = $\frac{\text{The reaction rate}}{\text{The amount of chemisorbed } H_2}$

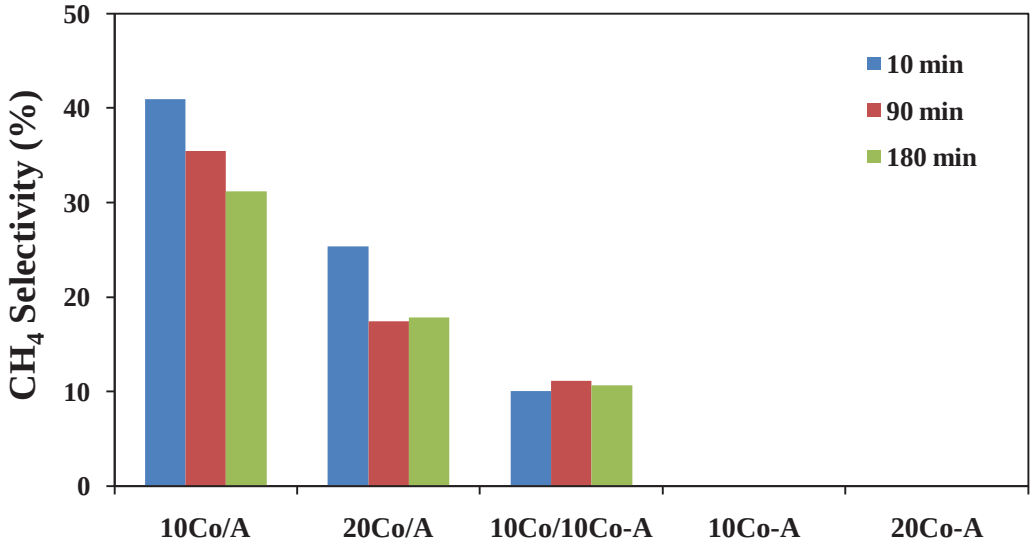

Figure 5.19 The CH_4 selectivity of FTS Co/Al_2O_3 catalyst

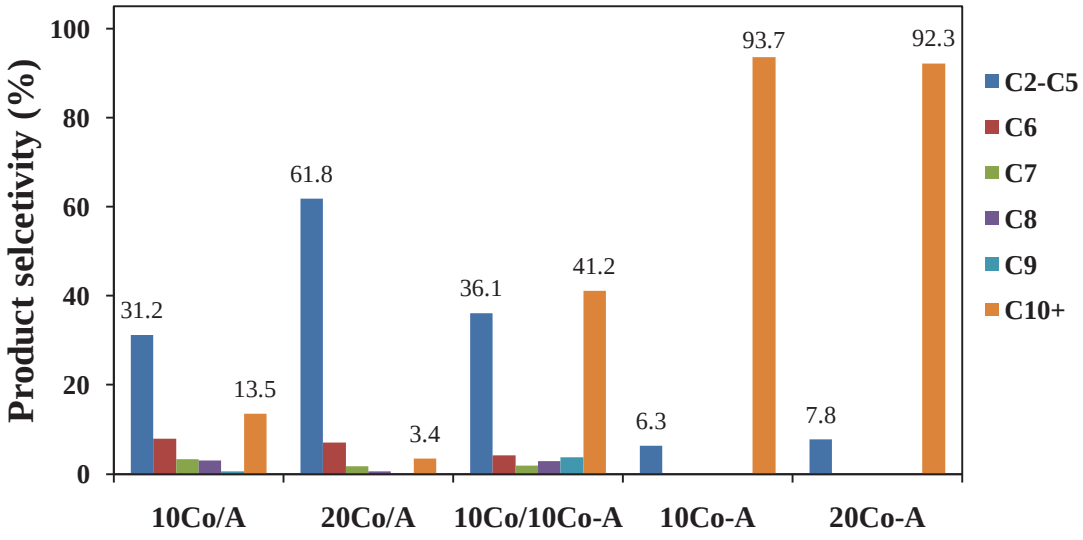

Figure 5.20 The product selectivity of FTS Co/Al_2O_3 catalyst at 10 min

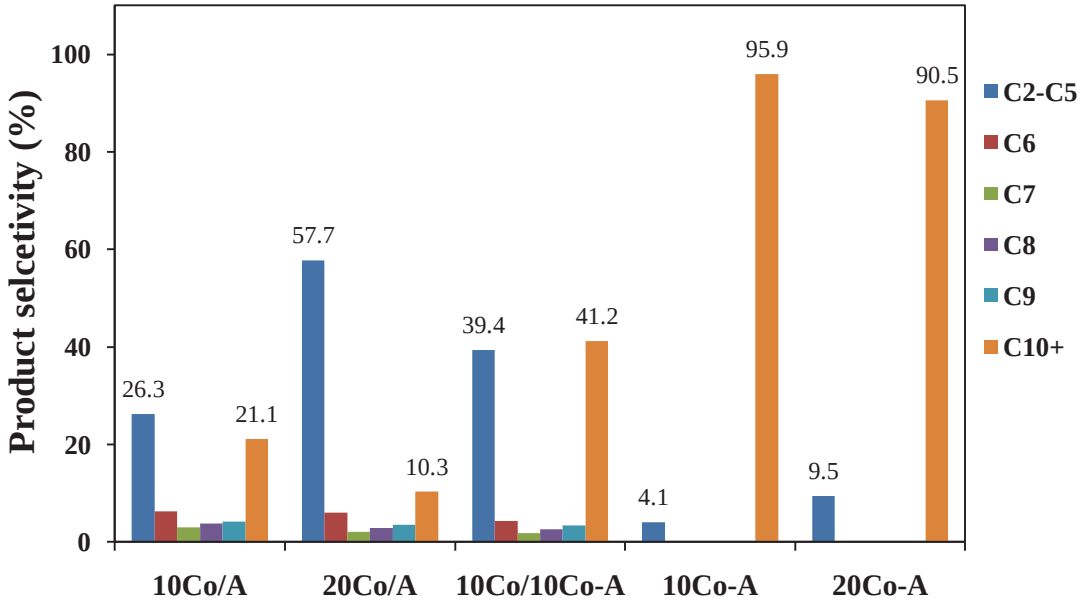

Figure 5.21 The product selectivity of FTS Co/Al_2O_3 catalyst at 90 min

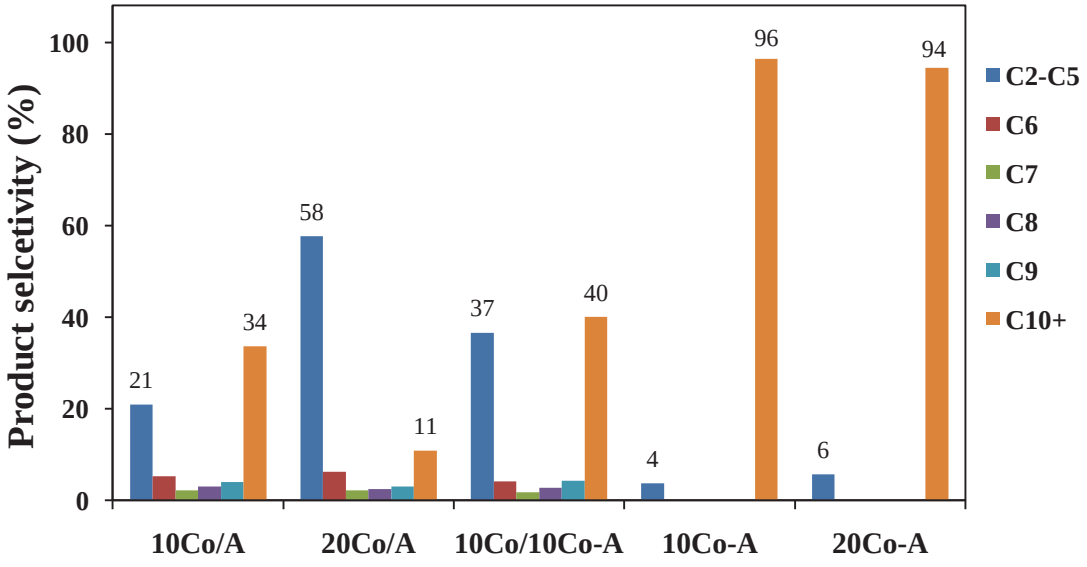

Figure 5.22 The product selectivity of FTS Co/Al_2O_3 catalyst at 180 min

5.3 Fischer-Trospch Synthesis Activity of Ru Loading

Table 5.7 shows the reaction rate and TOF for FTS of Co/Al_2O_3 catalyst with various Ru addition techniques at various times on stream. The presence of Ru on the 20Co/A catalyst shows higher the reaction rate and TOF than the absence of Ru. This resulted increasing the methane selectivity. The 0.5Ru/20Co-A and 20Co-0.5Ru-A showed the low reaction rate but the TOF cannot be determined because they gave very low Co active sites. The main products were the heavy hydrocarbons similar to the catalyst without Ru. The 10Co-0.5Ru/10Co-A had high reaction rate and TOF. It was remarked that the main products in this case were methane and light hydrocarbons. Figure 5.24 present the CH_4 selectivity of FTS Co/Al_2O_3 catalyst with various Ru loading methods and Figure 5.25-5.27 show the product selectivity of Co/Al_2O_3 catalyst with various Ru loading methods at various times on stream.

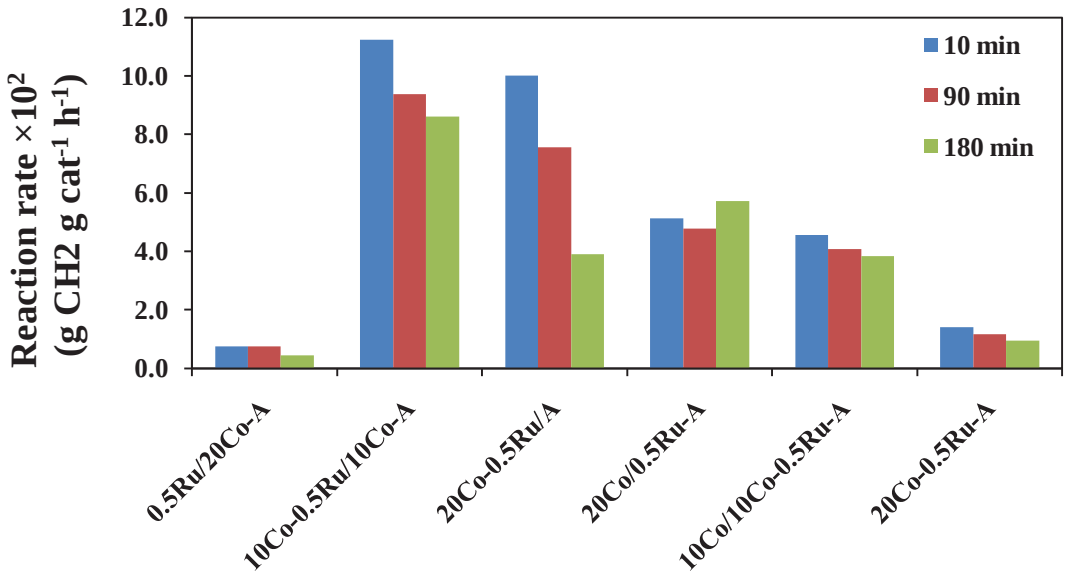

Figure 5.23 The reaction rate for FTS of Co/Al_2O_3 catalyst with various Ru loading methods

Table 5.7 The reaction rate and TOF for FTS of Co/Al_2O_3 catalyst with various Ru addition techniques

Catalysts	Time (min)	Reaction rate[a] $\times 10^2$ (g CH_2 $g_{cat}^{-1}h^{-1}$)	TOF[b] $\times 10^2$ (s^{-1})
0.5Ru/20Co-A	10	0.45	n.d.
	90	0.45	n.d.
	180	0.30	n.d.
10Co-0.5Ru/10Co-A	10	11.55	2.24
	90	9.37	1.81
	180	7.85	1.52
20Co-0.5Ru/A	10	10.01	1.27
	90	7.56	0.96
	180	3.89	0.49
20Co/0.5Ru-A	10	5.13	0.57
	90	4.78	0.53
	180	5.72	0.63
10Co/10Co-0.5Ru-A	10	4.56	0.86
	90	4.08	0.77
	180	3.84	0.72
20Co-0.5Ru-A	10	3.73	n.d.
	90	0.93	n.d.
	180	0.70	n.d.

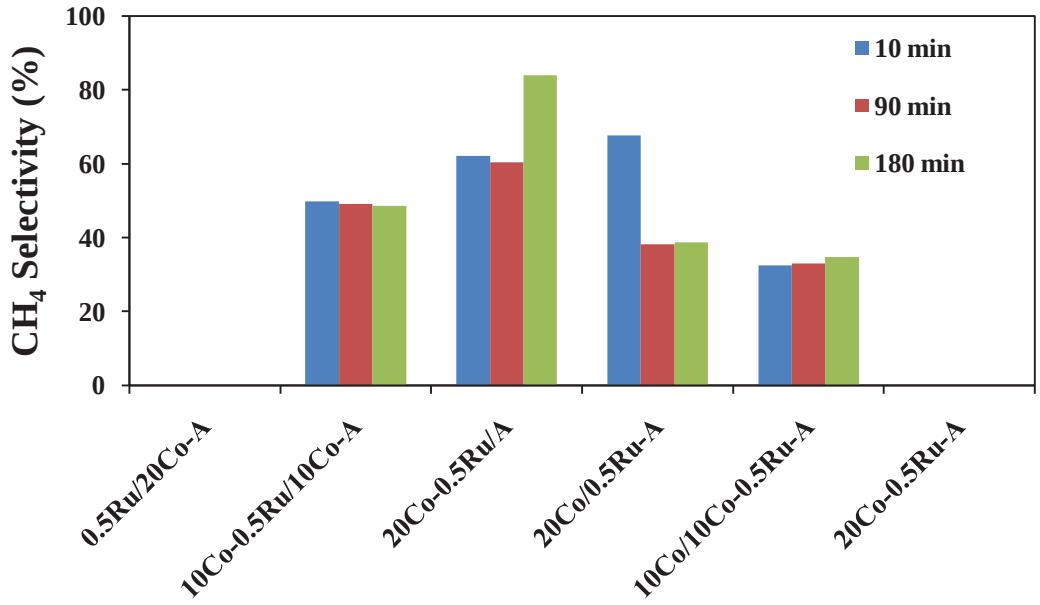

Figure 5.24 The CH_4 selectivity of FTS Co/Al_2O_3 catalyst with various Ru loading methods

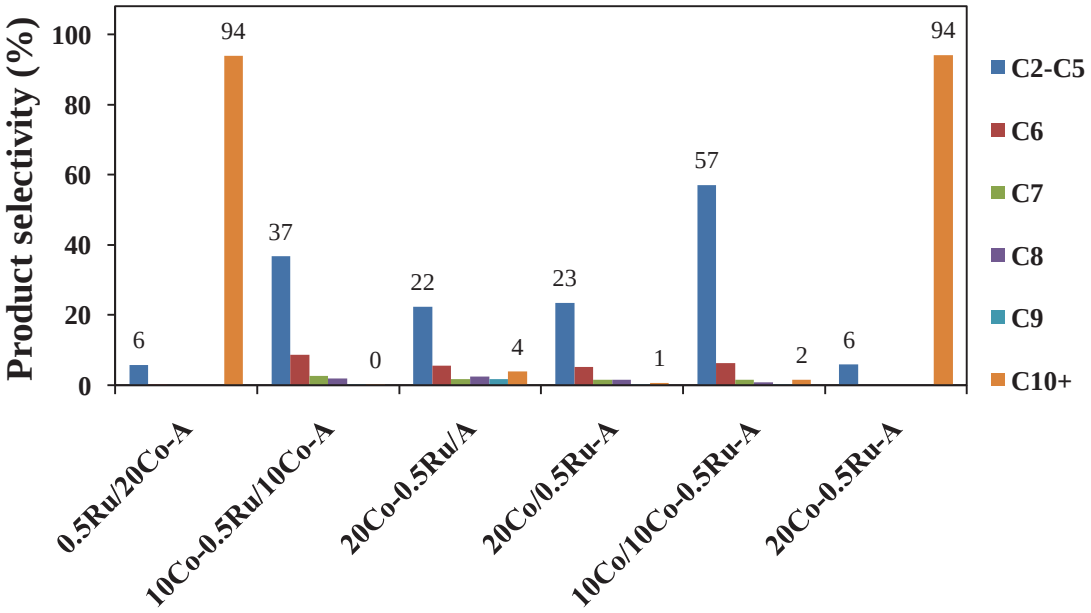

Figure 5.25 The product selectivity of FTS Co/Al_2O_3 catalyst with various Ru loading methods at 10 min

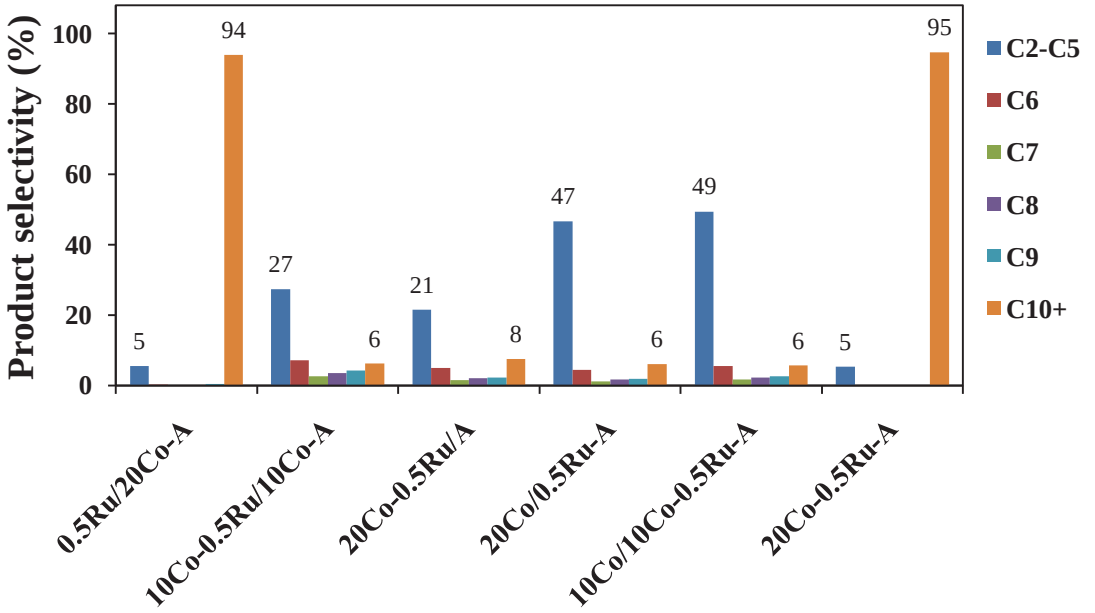

Figure 5.26 The product selectivity of FTS Co/Al_2O_3 catalyst with various Ru loading methods at 90 min

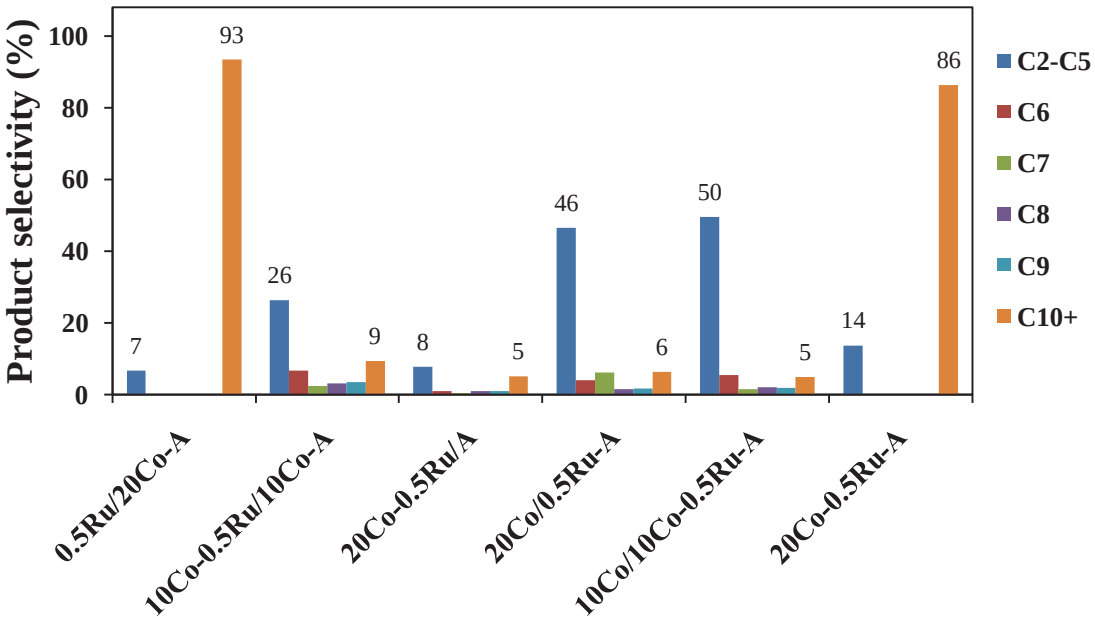

Figure 5.27 The product selectivity of FTS Co/Al_2O_3 catalyst with various Ru loading methods at 180 min

CHAPTER 6

CONCLUSIONS AND RECOMMENDATION

In this research, the catalytic performance of cobalt nanoparticle supported on Al_2O_3 catalyst using flame spray pyrolysis (FSP) technique and the effect of ruthenium promoter on the Fischer-Tropsch synthesis (FTS) were investigated. The experimental conclusions were summarized as follows:

1. FSP can synthesize the Al_2O_3 support, which contained three mixed phase of chi, gamma and alpha phases. The Co incorporated with Al_2O_3 by FSP can inhibit phase transformation of gamma to alpha phase.

2. Co incorporated with Al_2O_3 by FSP results in the formation of cobalt aluminate ($CoAl_2O_4$).

3. The Co-A and Co/A exhibited different catalytic behaviors. The Co-A prefers to the production of long chain hydrocarbons (C_{10+}) while the Co/A promoted the formation of methane and light hydrocarbons.

4. The 10Co/10Co-A shows a low reaction rate, but there is significant change in product selectivity leading to obtain the desired product.

4. Addition of Ru in the FSP catalyst increases Co_3O_4 reducibility and Co dispersion, resulting in higher FT activity.

5. The 10Co-0.5Ru/10Co-A gives the highest reaction rate and TOF. However, it is remarkable that the main products are methane (CH_4) and light hydrocarbons (C_2-C_5).

The recommendations for further study were suggested as follows:

1. The roles of cobalt aluminate on the FTS should be focused in many aspects.

2. The 10Co-05Ru/10Co-A catalyst should be developed to maintain a high of the reaction rate.

BIBLIOGRAPHY

[1] A. Bao, K. Liew, J. Li, *Fischer–Tropsch synthesis on CaO-promoted Co/Al_2O_3 catalysts*, **J. Mol. Catal. A: Chem.**, 304 (2009) 47–51

[2] M. Rønning, N. E. Tsakoumis, Alexey Voronov, R. E. Johnsen , P. Norby ,W. van Beek, Ø. Borg, E. Rytter, A. Holmen, *Combined XRD and XANES studies of a Re-promoted Co/ γ-Al_2O_3 catalyst at Fischer–Tropsch synthesis conditions*, **Catal. Today**, 155 (2010) 289–295

[3] K. Songoupakan, P. Kongthong, W. Phiwkliang, *Investigation of the catalytic performance of zirconia supported cobalt catalyst prepared by flame spray pyrolysis for the Fischer-Tropsch synthesis*, **Thesis (B.Eng.), Silpakorn University** (2007).

[4] A. Tavasoli, K. Sadagiani, F. Khorashe, A.A. Seifkordi, A.A.Rohani, A. Nakhaeipour, *Cobalt supported on carbon nanotubes-A promising novel Fischer-Tropsch synthesis catalyst*, **Fuel Process Technol.**, 89 (2008) 491-498

[5] O. Gonza´lez, H. Pe´rez , P. Navarro, L.C. Almeida, J.G. Pacheco, M. Montes, *Use of different mesostructured materials based on silica as cobalt supports for the Fischer-Tropsch synthesis*, **Catal. Today**, 148 (2009) 140–147

[6] X. Sun, X. Zhang, Y. Zhang, N. Tsubaki, *Reversible promotional effect of SiO_2 modification to Co/Al_2O_3 catalyst for Fischer–Tropsch synthesis*, **Appl. Catal. A: Gen.**, 377 (2010) 134–139

[7] S.H. Song, S.B. Lee, J.W. Bae, P.S. Prasad, K.W. Jun, *Influence of Ru segregation on the activity of Ru–Co/γ-Al_2O_3 during FT synthesis: A comparison with that of Ru–Co/SiO_2 catalysts*, **Catal. Commun.**, 9 (2008) 2282–2286.

[8] A. Sari, Y. Zamani, S.A. Taheri, *Intrinsic kinetics of Fischer-Tropsch reactions over an industrial Co–Ru/γ-Al_2O_3catalyst in slurry phase reactor*, **Fuel Process Technol.**, 90 (2009) 1305–1313

[9] R. Strobel, A. Baiker, S. E. Pratsinis, *Aerosol flame synthesis of catalysts*, **Adv. Powd. Technol.**, 17 (2006) 457–480

[10] R. Mueller, L. M-adler, S.E. Pratsinis, *Nanoparticle synthesis at high production rates by flame spray pyrolysis*, **Chem. Eng. Sci.**, 58 (2003) 1969-1976

[11] H. Xiong, Y. Zhang, S. Wang, J. Li, *Fischer–Tropsch synthesis: the effect of Al2O3 porosity on the performance of Co/Al_2O_3 catalyst*, **Catal. Commun.**, 6 (2005) 512–516

[12] H. Xiong, Y. Zhang, K. Liew, J. Li, *Catalytic performance of zirconium-modified Co/Al2O3 for Fischer–Tropsch synthesis*, **J. Mol. Catal. A: Chem.**, 231 (2005) 145–151

[13] T. Burakorn, J. Panpranot, O. Mekasuwandumrong, C. Chaisuk, P. Praserthdam, B. Jongsomjit, *Characterization of cobalt dispersed on the mixed nanoscale alumina and zirconia supports*, **J. Mater. Process Technol.**,206 (2008) 352

[14] A. Karimi, A. Nakhaei Pour, F. Torabi, B. Hatami, A. Tavasoli, M. Reza Alaei, M. Irani, Fischer-Tropsch synthesis over ruthenium-promoted Co/Al_2O_3 catalyst with different reduction procedures, **J. Natur Gas Chem.**, 19 (2010) 503–508

[15] S.A. Hosseini, A. Taeb, F. Feyzi, F. Yaripour. *Fischer–Tropsch synthesis Over Ru promoted Co/γ-Al_2O_3 catalysts in a CSTR*. **Catal. Commun.**, 5 (2004) 137-143.

[16] P. Li, J. Liu, N. Nag, P.A. Crozier, *In situ synthesis and characterization of Ru promoted Co/Al_2O_3 Fischer–Tropsch catalysts*, **Appl. Catal. A: Gen.**, 307 (2006) 212–221.

[17] R. Strobel, Sotiris E. Pratsinis, *Flame Synthesis of Supported Platinum Group Metals for Catalysis and Sensors*, **Platinum Metals Rev.**, 2009, **53**, (1), 11–20

[18] L. Mädler, H.K. Kammler, R. Mueller, S.E. Pratsinis, *Controlled synthesis of nanostructured particles by flame spray pyrolysis*, **J. Aerosol Sci.**, 33 (2002) 369.

[19] R. Strobel, A. Baiker, S.E. Pratsinis, *Aerosol flame synthesis of catalysts*, **Adv. Powder Technol.**, 17 (2006) 457–480

[20] M. Sokolowksi, A. Sokolowska, A. Michalski, B. Gokieli, *The 'in-flame-reaction' method for Al_2O_3 aerosol formation*, **J. Aerosol Sci.**, 8 (1977) 219.

[21] R. Strobel, Sotiris E. Pratsinis, *Flame aerosol synthesis of smart nanostructure materials*, **J. Mater. Chem.**, 17 (2007) 4743–4756

[22] R. Strobel, Frank Krumeich, Wendelin J. Stark, Sotiris E. Pratsinis, Alfons Baiker, *Flame spray synthesis of Pd/Al_2O_3 catalysts and their behavior in enantioselective hydrogenation*, **J. Catal**., 222 (2004) 307–314

[23] S.E. Pratsinis, *Flame aerosol synthesis of ceramic powders*, **Prog. Energy Combust. Sci.**, 24 (1998) 197.

[24] W.J. Stark, L. Mädler, M. Maciejewski, S.E. Pratsinis, A. Baiker, *Flame synthesis of nanocrystalline ceria-zirconia: effect of carrier liquid*, **Chem. Commu.**, (2003) 588.

[25] R. Strobel,W.J. Stark, L. M¨ldler, S.E. Pratsinis, A. Baiker, *Flame-made platinum/alumina: structural properties and catalytic behaviour in enantioselective hydrogenation*, **J. Catal.**, 213 (2003) 296.

[26] H. Chang, S.J. Kim, H.D. Jang, J.W. Choi, *Synthetic routes for titania nanoparticles in the flame spray pyrolysis*, **Colloids Surf A: Physicochem. Eng. Aspects**, 313 (2008) 282.

[27] H. Chang, J.H. Park, H.D. Jang, *Flame synthesis of silica nanoparticles by adopting two-fluid nozzle spray*, **Colloids Surf A: Physicochem. Eng. Aspects**, 313 (2008) 140.

[28] Laan, G.P. van der, *Kinetics, selectivity and scale up of the Fischer-Tropsch synthesis,chapter 2, Kinetics and selectivity of the Fischer-Tropsch Synthesis. A Literature review*, **Thesis university of Groningen**, (1999).

[29] Henricus A.J. van Dijk, *The Fischer-Tropsch synthesis: A mechanistic study using transient isotopic tracing*, **Thesis of Technische Universiteit Eindhoven**, (2001).

[30] M.J. Overett, R.O. Hill, J.R. Moss, *Organometallic chemistry and surface science mechanistic models for the Fischer–Tropsch Synthesis*, **Coor. Chem. Rev.**, 206 (2000) 581.

[31] M.E. Dry, *Practical and theoretical aspects of the catalytic Fischer-Tropsch process*, **App. Cat. A: Gen.**, 138 (1996) 319.

[32] R. George, J.M. Andersen, J.R. Moss, *A comparison of the rates of alkyl migration in the complexes [CpM(CO)$_2$R](M=Fe, Ru, Os; Cp = η^5-C$_5$H$_5$)*, **J. Organomet. Chem.**, 505 (1995) 131.

[33] X. Yin, J.R. Moss, *Synthesis and characterization of long chain acyl and alkyl complexes of the types [(η^5-C$_5$R'$_5$)Fe(CO)$_2${C(O)R}] (R'=H, CH$_3$), [CpW(CO)$_3${C(O)R}] and [CpW(CO)$_3$R] (R=n-alkyl)*, **Inorg. Chem. Acta.**, 286 (1999) 221.

[34] M.E. Dry, *The Fischer–Tropsch process: 1950-2000*, **Catal. Today**, 71 (2002) 227.

[35] M.A. Vannice, *The catalytic synthesis of hydrocarbons from H$_2$/CO mixtures over the group VIII metals: I. The specific activities and product distributions of supported metals*, **J. Catal.**, 37 (1975) 449.

[36] E. Iglesia, S.L. Soled, R.A. Fiato, *Fischer-Tropsch synthesis on cobalt and ruthenium. Metal dispersion and support effects on reaction rate and selectivity*, **J. Catal.**, 137 (1992) 212.

37] I. Puskas, R.S. Hurlbut, *Comments about the causes of deviations from the Anderson-Schulz-Flory distribution of the Fischer-Tropsch reaction products*, **Catal. Today**, 84 (2003) 99.

[38] C. H. Bartholomew, R. J. Farrauto, *Fundamentals of Industrial Catalytic Processes*, 2nd edition, Wiley, (2005) 398.

[39] J. Patzlaff, Y. Liu, C. Graffmann, J. Gaube, *Interpretation and kinetic modeling of productdistribution of cobalt catalyzed Fischer-Tropsch synthesis*, **Catal. Today**, 71 (2002) 381.

[40] R. Parichart, P. Somjit, F.Anusara, *Investigation of the cobalt incorporation and ruthenium addition in zirconia supported cobalt catalyst for the Fischer-Tropsch synthesis*, **Thesis (B.Eng.), Silpakorn University**, (2008).

[41] N. Kiattisak, A. Ratchakorn, P. Uraiwan, *Modification of alumina support of platinum-tin catalyst for n-heptane reforming*, **Thesis (B.Eng.), Silpakorn University**, (2007).

[42] J. Panpranot, J.G. Goodwing Jr., A. Sayari, *Synthesis and characteristics of MCM-41 supported CoRu catalysts*, **Catal. Today**, 77 (2002) 269.

[43] J. Panpranot, J.G. Goodwin, A. Sayari, *CO Hydrogenation on Ru-Promoted Co/MCM-41 Catalysts*, **J. Catal.**, 211 (2002) 530.

[44] G.K. Chuah, S. Jaenicke, B.K. Pong, *The Preparation of High Surface-Area Zirconia II. Influence of Precipitating Agent and Digestion on the Morphology and Microstructure of Hydrous Zirconia*, **J. Catal.**, 175 (1998) 80.

[45] Y. Liu, J. Chen, K. Fang, Y. Wang, Y. Sun, *A large pore-size mesoporous zirconia supported cobalt catalyst with good performance in Fischer-Tropsch synthesis*, **Catal. Commun.**, 8 (2007) 945.

[46] D.I. Enache, M. Roy-Auberger, R. Revel, *Differences in the characteristics and catalytic properties of cobalt-based Fischer-Tropsch catalysts supported on zirconia and alumina*, **Appl. Catal. A: Gen.**, 268 (2004) 51.

[47] W.Y. Teoh, R. Setiawan, L. Madler, J.D. Grunwaldt, R. Amal, S.E. Pratsinis, *Ru-dope cobalt-zirconia nanocomposites by flame synthesis: physicochemical and cayalytic properties*, **Chem. Mater.**, 20 (2008) 4069-4079

[48] Seon-Ju Park, J.W. Bae, Jong-Hyeok Oh, K.V.R. Chary, P.S. Sai Prasad, Ki-Won Jun, Young-Woo Rhee, *Influence of bimodal pore size distribution of Ru/Co/ZrO_2–Al_2O_3 duringFischer–Tropsch synthesis in fixed-bed and slurry reactor*, **J. Mol. Catal. A: Chem.**, 298 (2009) 81–87

[49] R.C. Reuel, C.H. Bartholomew, *Effects of support and dispersion on the CO hydrogenation activity/selectivity properties of cobalt*, **J. Catal.**, 85 (1984) 78.

[50] J. Xiong, O. Borg, E. Anders Blekkan, A. Holmen, *Hydrogen chemisorption on rhenium-promoted c-alumina supported cobalt catalysts*, **Catal. Commun.**, 9 (2008) 2327–2330

[51] I. Mindru, G. Marinescu, D. Gingasu, L. Patron, C. Ghica, M. Giurginc, *Blue $CoAl_2O_4$ spinel via complexation method*, **Mater. Chem. Phys**., 122 (2010) 491–497

[52] F. Yu, J. Yang, J. Ma, J. Du, Y. Zhou, *Preparation of nanosized $CoAl_2O_4$ powders by sol–gel and sol–gel-hydrothermal methods*, **J. Alloys Compd.**, 468 (2009) 443–446

APPENDIX

APPENDIX A

APPENDIX A

CALCULATION FOR CATALYST PREPARATION

Table A.1 Chemical Properties

Metal or Metal oxide	MW of metal	Metal Precursor	MW of Metal Precursor	Density (g/cm^3)	Metal content (%)
Co	58.93	$Co(C_{11}H_{10}O_2)_2$	407.25	0.92	10
Co	58.93	$Co(NO_3)_2.6H_2O$	291.03	-	-
Al_2O_3	101.96	$Al(OCH(CH_3)C_2H_5)_3$	246.33	0.96	97

A.1 Calculation of catalyst prepared by wet impregnation

Preparation of catalysts by wet impregnation method is shown as follows:

Reagent: 20 wt% Co of Cobalt nitrate [$Co(NO_3)_2 \cdot 6H_2O$]

Support: Al_2O_3

Example: Calculation for the preparation of 20Co/A catalyst with $Co(NO_3)_2 \cdot 6H_2O$ as Co precursor

Based on 100 g of catalyst used, the composition of the catalyst will be as follows:

Co = 20 g

Al_2O_3 = 100-20 = 80 g

For 2 g of catalyst

Cobalt required = 2 × (20/80) = 0.50 g

Thus, Cobalt 0.50 g was prepared from Cobalt nitrate

Cobalt metal 58.93 g in Cobalt nitrate 291.03 g

For 0.5 g of cobalt metal

Cobalt nitrate required = 0.5 × (291.03/58.93) = 2.47 g

A.2 Calculation of catalyst prepared by flame spray pyrolysis

0.5 M solution was used as precursor for catalyst preparation by flame spray pyrolysis is shown as follows:

Example: Calculation for the preparation of the 20Co-A catalysts, Aluminium-tri-sec-butoxide [$Al(OCH(CH_3)C_2H_5)_3$] (Sigma-Aldrich) and cobalt naphthenate [$Co(C_{11}H_{10}O_2)_2$] (Fluka) were used as precursor and diluted with xylene (Sigma-Aldrich) to a 0.5 M solution.

Based on 0.5 M solution 20 wt%Co/Al_2O_3 used, the composition of the catalyst will be as follows:

$$\textit{Cobalt} = 20\ g \qquad \textit{Al}_2\textit{O}_3 = 100 - 20 = 80\ g$$

Mole Fraction:

$$Co = 20\ g\ Co \left| \frac{1\ mol\ Co}{58.93\ g\ Co} \right. = 0.3394\ mol\ Co$$

$$Al = 80\ g\ Al_2O_3 \left| \frac{1\ mol\ Al_2O_3}{101.96\ g\ Al_2O_3} \right| \frac{2\ mol\ Al}{1\ mol\ Al_2O_3} = 1.5692\ mol\ Al$$

$$\therefore\ Total\ Mole\ Fraction = 0.3394 + 1.5692 = 1.9086\ mol$$

Basis 500 ml precursor solution 0.5 M: $$200\ ml \left| \frac{0.5\ mol}{1000\ ml} \right. = 0.25\ mol$$

$$mol\ Co: \quad 0.25\ mol \left| \frac{0.3394\ mol\ Co}{1.9086\ mol} \right. = 0.0445\ mol\ Co$$

$$mol\ Al: \quad 0.25\ mol \left| \frac{1.5692\ mol\ Al}{1.9086\ mol} \right. = 0.2055\ mol\ Al$$

$$\therefore Co\ precursor = 0.0445\ mol\ Co \left| \frac{58.93\ g\ Co\ precursor}{1\ mol\ Co} \right| \frac{1\ ml}{0.92\ g} \left| \frac{1}{0.1} \right. = 28.476\ ml\ Co$$

$$\therefore Al\ precursor = 0.2055\ mol\ Al \left| \frac{246.33\ g\ Al\ precursor}{1\ mol\ Al} \right| \frac{1\ ml}{0.96\ g} \left| \frac{1}{0.97} \right. = 54.3723\ ml\ Al$$

APPENDIX B

APPENDIX B

CALCULATION OF THE CRYSTALLITE SIZE

Calculation of the crystallite size by Debye-Scherrer equation

The crystallite size was calculated from the half-height width of the diffraction peak of XRD pattern using the Debye-Scherrer equation.

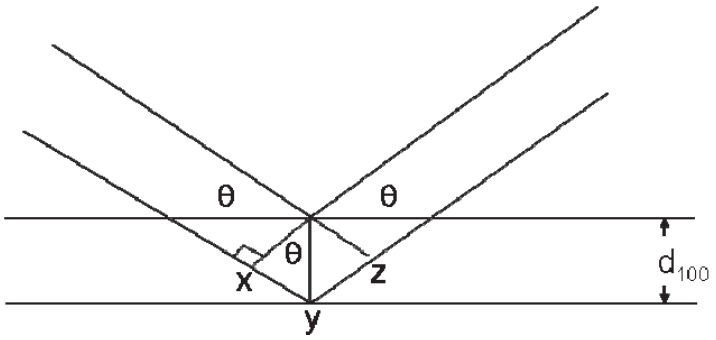

Figure B.1 Derivation of Bragg's Law for X-ray diffraction

$$xy = yz = d\sin\theta$$

Thus $xyz = 2d\sin\theta$

But $xyz = n\lambda$

Therefore $2d\sin\theta = n\lambda$ *Bragg's Law*

$$d = \frac{n\lambda}{2\sin\theta}$$

The Bragg's Law was derived to B.1

From Scherrer equation:

$$D = \frac{K\lambda}{\beta\cos\theta} \qquad (B.1)$$

Where D = Crystallite size, Å

K = Crystallite-shape factor = 0.9

λ = X-ray wavelength, 1.5418 Å for CuKα

θ = Observed peak angle, degree

β = X-ray diffraction broadening, radian

The X-ray diffraction broadening (β) is the pure width of powder diffraction free from all broadening due to the experimental equipment. α-alumina is used as a standard sample to observe the instrumental broadening since its crystallite size is larger than 2000 Å. The X-ray diffraction broadening (β) can be obtained by using Warren's formula.

From Warren's formula:

$$\beta = \sqrt{B_M^2 - B_S^2} \qquad (B.2)$$

Where B_M = The measured peak width in radians at half peak height.

B_S = The corresponding width of the standard material.

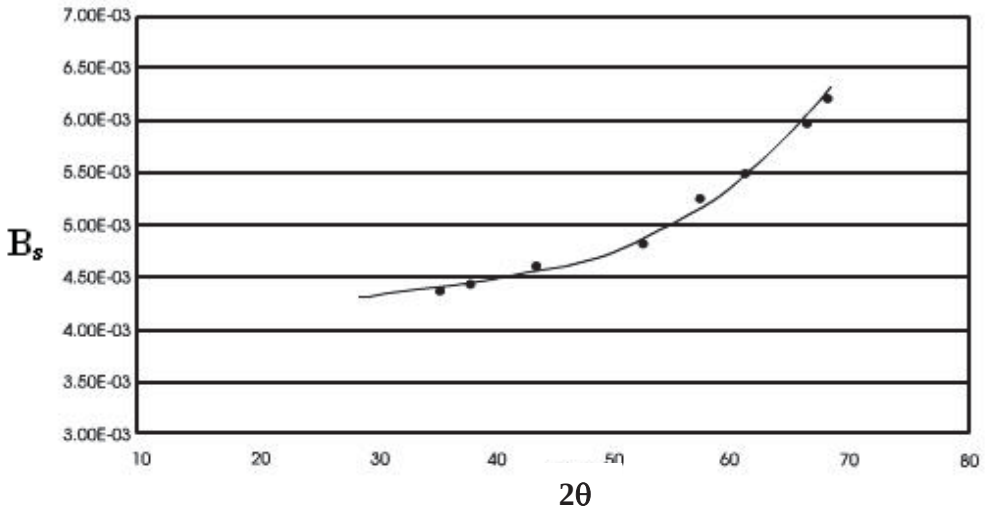

Figure B.2 The plot indicating the value of line broadening due to the equipment. The data were obtained by using α-alumina as a standard

APPENDIX C

APPENDIX C

CALCULATION FOR REDUCIBILITY

For supported cobalt catalyst, it can be assumed that the major species of calcined Co catalysts is Co_3O_4. H_2 consumption to reduce Co_3O_4 is calculated as follows:

Molecular weight of Co = 58.93

Molecular weight of Co_3O_4 = 240.79

Calculation of the calibration of H_2 consumption using cobalt oxide (Co_3O_4)

Let the weight of Co_3O_4 used = 0.1 g

= 4.153×10^{-4} mole

From equation of Co_3O_4 reduction;

$Co_3O_4 + 4H_2 \rightarrow 3Co + 4H_2O$ *(E.1)*

Mole of hydrogen consumption = 4 Mole of Co_3O_4 consumption

= $4\times4.153\times10^{-4}$

= 1.661×10^{-3} mole

Integral area of hydrogen used to reduce Co_3O_4 0.1 g = 7.5 unit

At 100 % reducibility, the amount of hydrogen consumption is 1.661×10^{-3} mole related to the integral area of Co_3O_4 after reduction 7.5 unit.

Calculation of reducibility of supported cobalt catalyst

$$\%\,\text{Reducibility} = \frac{\text{Amount of } H_2 \text{ uptake to reduce 1 g of catalyst} \times 100}{\text{Amount of theoretical } H_2 \text{ uptake to reduce } Co_3O_4 \text{ to } Co^0 \text{ for 1 g of catalyst}}$$

Integral area of the calcined catalyst = X unit

The amount of H_2 consumption = $\left[2\times1.661\times10^{-3}\times(X)/115.63\right]$mole

Let the weight of calcined catalyst used = W g

Concentration of Co = Y %wt

Mole of Co = $\left[(\mathrm{W}\times\mathrm{Y}/100)/58.93\right]$ mole

Mole of Co_3O_4 = $\left[(\mathrm{W}\times\mathrm{Y}/100)/(3\times58.93)\right]$ mole

Amount of theoretical = $\left[(\mathrm{W}\times\mathrm{Y}/100)\times4/(3\times58.93)\right]$mole

Reducibility (%) of supported Co catalyst = $\dfrac{\left[2\times1.661\times10^{-3}\times(X)/115.63\right]\times100}{\left[(W\times Y/100)\times4/(3\times58.93)\right]}$

APPENDIX D

APPENDIX D

CALCULATION FOR TOTAL H_2 CHEMISORPTION AND DISPERSION

Calculation of the total H_2 chemisorption and metal dispersion of the catalyst, a stoischiometry of H_2 : Co = 1 : 2, is assumed. The calculation procedure is as follows:

Let the weight of catalyst used	=	W	g
Integral area of H_2 peak after adsorption	=	A	unit
Integral area of 100 μl of standard H_2 peak	=	B	unit
Amounts of H_2 adsorbed on catalyst	=	B-A	unit
Concentration of Co	=	20	%wt
Volume of H_2 adsorbed on catalyst	=	100 × [(B-A)/B]	μl
Volume of 1 mole of H_2 at 100 °C	=	29.93×10^{6}	μl

Mole of H_2 adsorbed on catalyst = [(B-A)/B]×[100/29.93] μmole

Total hydrogen chemisorption = [(B-A)/B]×[100/29.93]×[1/W] μmole /$g_{catalyst}$

= N μmole /$g_{catalyst}$

$$\%Co\ dispersion = \frac{\text{The amount of cobalt equivalent to } H_2 \text{ adsorption after reduction}}{\text{Total amount of cobalt active sites expected to exist after reduction}} \times 100$$

Molecular weight of cobalt = 58.93

Metal dispersion (%) = $\dfrac{2\times H_{2\,tot}\times 100}{\text{No.}\,\mu\text{mole}\,Co_{tot}}$

= $\dfrac{2\times N\times 100}{\text{No.}\,\mu\text{mole}\,Co_{tot}}$

= $\dfrac{2\times N\times 100}{\left[(\%reducibility/100)\times 0.10\times(0.2/58.93)\times 10^{6}\right]}$

= $\dfrac{200\times N}{(\%reducibility/100)\times 339.39}$

APPENDIX E

APPENDIX E

CALCULATION OF CO CONVERSION, REACTION RATE AND SELECTIVITY

The catalyst performance for the Fischer Tropsch synthesis was evaluated in terms of activity for CO conversion reaction rate and selectivity.

Activity of the catalyst performed in term of carbon monoxide conversion and reaction rate. Carbon monoxide conversion is defined as moles of CO converted with respect to CO in feed:

$$\text{CO conversion (\%)} = \frac{[\text{area of CO in feed} - \text{area of CO in product}] \times 100}{\text{area of CO in feed}} \qquad (F.1)$$

Which area of CO obtained from computer program based plot on TCD (GC-14B).

Reaction rate was calculated from CO conversion that is as follows:

Let the weight of catalyst used	*= W*	*g*
Flow rate of CO	*= 9*	*ml/min*
Reaction time	*= 60*	*min*
Weight of CH_2	*= 14*	*g*
Volume of 1 mole of gas at 1 atm	*= 24450*	*ml*

Reaction rate (g CH_2 / g of catalyst / h)

$$= \frac{[\%\ conversion\ of\ CO/100] \times 60 \times 14 \times 9}{W \times 24450} \qquad (F.2)$$

$$= A \quad g\ CH_2 / g\ of\ catalyst / h$$

Selectivity of product is defined as weight of product (B) form with respect to total area of product:

$$\text{Selectivity of B (wt \%)} = 100 \times [\text{area of B form} / \text{total area of product}] \qquad (F.3)$$

Which area of product obtained from computer program based plot FID (GC-14B).

APPENDIX F

APPENDIX F

INTERNATIONAL PROCEEDING

Naphaphan Kunthakudee*, Choowong Chaisuk and Kajornsak Faungnawakij

"Development of cobalt nanoparticle catalyst using flame spray pyrolysis technique for production of synthetic fuel by Fischer-Tropsch synthesis", 17th Regional Symposium on Chemical Engineering (RSCE), Thailand, 22-23 Nov, 2010 (oral presentation)

BIOGRAPHY

Name-Family name Miss Naphapan Khuntakudee

Birthd May 17, 1987 in Chachoengsao, Thailand.

Address 33 Nongrong District, Nongkhae Amphur, Saraburi Province, Thailand, 18140.

Education Background

2008 received the bachelor degree of Chemical Engineering, Faculty of Engineering and Industrial Technology, Silpakorn University, Nakhon Phathom, Thailand.

2010 further studied in the master degree of Engineering, Department of Chemical Engineering, Graduate School, Silpakorn University, Thailand.

Special Interest Nanoparticles/Aerosol Technology/Heterogeneous Catalysis